Supporting Information for "Investigating Mesozoic Climate Trends and Sensitivities with a Large Ensemble of Climate Model Simulations"

Jan Landwehrs[1,2], Georg Feulner[2], Stefan Petri[2], Benjamin Sames[1] and Michael Wagreich[1]

[1]Department of Geology, University of Vienna, Althanstraße 14, 1090 Vienna, Austria

[2]Earth System Analysis, Potsdam Institute for Climate Impact Research, Member of the Leibniz Association, P.O. Box 601203, D-14412 Potsdam, Germany

Contents of this file

1. Sections 1–10
2. Table S1
3. Figures S1–S22

Additional Supporting Information (Files uploaded separately):
See data repository at

`https://doi.org/10.5880/PIK.2020.009`

Corresponding author: J. Landwehrs, jan.landwehrs@univie.ac.at

February 5, 2021, 7:43pm

1. Boundary Conditions: Orography, Bathymetry and Vegetation (Figs. S1–S3)

The topography (see Fig. S1) and bathymetry (see Fig. S2) implemented in the model simulations are based on the paleogeographic reconstructions of Scotese and Wright (2018). After interpolating onto the ocean model grid, the following necessary adjustments were made: Narrow straits with less than two grid cell widths were closed or widened. Isolated ocean cells needed to be removed or connected to the global ocean. To improve model stability, the minimum ocean depth was increased to 461 m and the upper-/lowermost grid row were set to a uniform median depth. Also, random variations of the deepest sea floor were introduced where it was completely flat in the original elevation model. The adjustments were kept as small and consistent as possible. As this study assesses global scale surface climates over a long geological time span, it was beyond the scope of this work to review specific features like ocean gateway configurations with regard to proxy evidence. Given the uncertainties in the paleogeographic reconstructions itself, such a review would certainly be warranted when focusing on the connection between tectonic changes, ocean circulation and climate for specific time periods and geographical regions.

For Fig. 4 and Fig. 7b, locations at the respective timeslice were reconstructed with pyGPlates using the data and the (Scotese, 2008) paleorotation model provided by (Cao et al., 2018). For Fig. 7b, the occurrences were sampled on the $3.75 \times 3.75\,^{\circ}$ grid and the size of the triangles scales with the frequency of the occurrences on this grid. Because the paleogeography changes within the relatively broad time-bins of the proxy data, the locations show a certain drift for timeslices within these time-bins.

2. Spin-Up (Figs. S4–S6)

Fig. S4 shows GMST timeseries (Fig. S4 during the 5000 yr spin-up for all simulations.

For a subset of runs ($\mathtt{P}_{\mathtt{pCO2\_1000ppm}}$ for $\mathtt{T}_{\mathtt{25Myr}}$), Fig. S6 shows global mean ocean seawater temperature and salinity at different depths over time.

For the same subset, Fig. S5 shows the relation of global mean top-of-the-atmosphere radiation balance (RBTP) and GMST during spin-up.

Fig. S6 shows global mean seawater temperature and salinity at three depth levels during spinup.

Similar plots for each individual run are included in the accompanying data repository (AllRuns_Spinup.pdf).

3. Atmosphere Fields (Figs. S7–S11)

Figures S7 to S10 illustrate the simulated surface air temperatures, precipitation and surface radiation balance for the four exemplary timeslices 75, 125, 175 and 225 Ma presented in the main article figures (similar maps for all simulation runs are included in the data repository). Figure S11 indicates the simulated change of precipitation and the surface radiation balance on land through time.

4. Global Mean Sea-Level Temperatures (Fig. S12)

Fig. S12 shows simulated global mean surface air temperatures compared to lapse-rate corrected global mean temperatures at sea-level for the $\mathtt{P}_{\mathtt{pCO2\_1000ppm}}$ and the $\mathtt{P}_{\mathtt{VegFix\_S0ini}}$ pathways.

5. Correlation of Global Mean Temperatures with the Total Area and Distribution of Land (Fig. S13)

Fig. S13 shows the correlation of lapse-rate corrected global mean air temperatures at sea level ($\mathrm{GMT_{SL}}$) with the global land area fraction (a) and the average absolute latitude of land area (b). For the simulations of the $\mathtt{P}_{\mathtt{VegFix\_S0ini}}$ pathway.

6. Proxy and Model Temperature Estimates (Figs. S14–S15)

Climate models inherently yield self-constrained global temperature fields, but might miss important processes that shaped these in reality. Proxy approaches often aim to compile consistent and globally distributed datasets to generate meridional or global SST or SAT distributions to obtain GMST estimates. Retrieving and calibrating such datasets is challenging and converting them into GMSTs is non-trivial. For example, the GMST estimates from (Mills et al., 2019, Fig 4b) (also see Fig. 1c of the present article) were mainly obtained from reconstructed tropical SST anomalies via a scaling factor of 1.5 (Mills et al., 2019):

$$\Delta\mathrm{GMST} = \mathrm{GMST_{ref}} + 1.5 \cdot \Delta\mathrm{SST_{trop}} \tag{1}$$

Where $\mathrm{GMST_{ref}} = 15\,^{\circ}\mathrm{C}$ and $\Delta\mathrm{SST_{trop}} = -4.55 \cdot \delta^{18}\mathrm{O_{trop}}$ (Mills et al., 2019).

We tested the correlation of $\mathrm{SST_{trop}}$ and GMST (see Fig. S14a) in our model ensemble and indeed found an overall solid linear relationship (see Fig. S15a). However, we obtain a scaling factor of ∼1.79, indicating a stronger amplification of temperature changes at higher latitudes. Our results also suggest that the scaling is slightly higher for cooler climate states (see Fig. S15b), which could to some extent explain its variation through geologic time (Fig. S15c). For the latter panel, the correlation was calculated separately for the 9 $\mathtt{T}_{\mathtt{25Myr}}$ timeslices and their climate states at $\mathrm{pCO_2}$ =

[250, 500, 1000, 1500, 2000, 4000] ppm. The 75 Ma timeslice, which is warm-biased by other boundary conditions (e.g. S_0, paleogeography), exhibits a slightly smaller scaling factor compared to the cold-biased 200 Ma timeslice (Fig. S15c, see inset).

Using the mean scaling factor of 1.79 and a reference GMST of 15 °C (as in Mills et al., 2019), we can calculate tropical SST anomalies for our simulations (Fig. S14b). These can be compared with the results from (Mills et al., 2019). (For this, we had to scale their GMST envelope back to ΔSST_{trop} via Eq. 1, as the authors did not report the underlying low-latitude SST anomalies in the same form.) As described in Sec. 3.1 of the paper, there appears to be a qualitative agreement on a slight cooling towards the end-Triassic to Early Jurassic, a warming towards the mid-Cretaceous, and a cooling at the end of the Cretaceous. However, the proxy estimates of ΔSST_{trop} are amplified by a factor of 2 or 3 compared to those in our model (note the different y-axis scales in Fig. S14b). As discussed, this can have several reasons, including a too low model climate sensitivity or uncertainties in the proxy temperature calibration. In future work, we aim at more comprehensive proxy–model comparisons than could be achieved within the framework of this study.

7. Meridional Temperature Gradients (Figs. S16–S17)

Simulated zonal mean SAT and SST profiles for the 95 and 125 Ma timeslices are shown in Fig. S16 for comparison with Laugié et al. (2020) and Steinig et al. (2020) as discussed in the main text (Sec. 4). Similar plots for all timeslices are included in the accompanying data repository. The figures also indicate numerical values of the global, low latitude (<30 °), high latitude (>60 °) averages and the difference between the latter two (upper left corner). As in Laugié et al. (2020) the meridional temperature gradient was also determined as the average change in °C per °lat. via a linear regression between 30 and 80 ° latitude (upper right corner). The figures also include zonal mean temperatures calculated from model output from Valdes, Scotese, and Lunt (2020) and Farnsworth et al. (2019a).

For comparison with Fig. 5, zonal mean SAT and low–high latitude SAT differences are shown for data from Valdes et al. (2020) and Farnsworth et al. (2019a) in Fig. S17.

8. Meridional Heat Transport (Fig. S18)

Fig. S18 shows the change of the zonal and global mean meridional atmospheric/ocean/total heat transport through time. On a global average, the MHT varies less than ±0.2 PW around ∼2.6 PW between all simulations. It tends to be increased in cooler states, for low-obliquity orbital configurations (which are also cooler) and for homogeneous vegetation patterns. Three phases with relative strengthening ocean MHT in the northern (until ∼220 Ma), southern (∼220–110 Ma) and again northern (∼110–60 Ma)

hemisphere can be identified. To some degree, these periods also appear to coincide to with enhanced overturning (see Fig. S19 and AllRuns_OceanCrossections.pdf) and mixing in the respective hemisphere (see Fig. S21).

9. Ocean Fields (Figs. S19–S21)

Fig. S19 include meridional ocean cross-sections showing the annual mean ocean temperatures as a zonal mean, at 180 °W and 60 °E. They also show the global mean meridional overturning streamfunction. Similar plots for every simulation of the whole ensemble are included in the data repository (AllRuns_OceanCrosssections.pdf).

Fig. S20 show annual mean sea surface temperatures, surface salinity and mixed layer depth for simulations of the $\texttt{P}_{\texttt{pCO2\_1000ppm}}$ pathway. Similar plots for every simulation of the whole ensemble are included in the data repository (AllRuns_Maps.pdf).

Fig. S21 shows the zonal and annual mean mixed layer depth through time, aggregated for the $\texttt{P}_{\texttt{pCO2\_1000ppm}}$ pathway.

10. Seasonality (Fig. S22)

The same analysis of continental SAT seasonality as presented in Sec. 3.2 of the main paper was performed with modeling results from Valdes et al. (2020) and Farnsworth et al. (2019a) (see Fig. S22).

11. Table of runs

Table S1: List of all equilibrium climate simulations included in the analyses.

	Run	Age (Ma)	pCO_2 (ppm)	pCO_2 pathway	S_0 (W/m^2)	Land fraction (%)	T_{ann} (°C)	PRC_{ann} (mm/a)	$T_{ann,trend}$ (°C/500yrs)	Radiation imbalance (W/m^2)
0	060Ma_400ppm	60	400	proxy	1354.7	31.7	16.7	1022	0.015	0.042
1	060Ma_500ppm	60	500	COPSE	1354.7	31.7	17.7	1059	-0.044	0.065
2	060Ma_1000ppm	60	1000		1354.7	31.7	20.6	1178	0.002	0.022
3	065Ma_250ppm	65	250		1354.1	31.3	14.7	954	0.003	0.033
4	065Ma_300ppm	65	300	proxy	1354.1	31.3	15.5	984	-0.003	0.028
5	065Ma_500ppm	65	500		1354.1	31.3	17.7	1070	0.000	0.035
6	065Ma_600ppm	65	600	COPSE	1354.1	31.3	18.5	1101	0.003	0.022
7	065Ma_1000ppm	65	1000		1354.1	31.3	20.7	1188	-0.004	0.04
8	065Ma_1000ppm_S0ini	65	1000		1332.7	31.3	18.8	1101	-0.057	0.027
9	065Ma_1000ppm_S0ini_VegFix	65	1000		1332.7	31.3	18.8	1092	0.006	0.013
10	065Ma_1000ppm_VegHom	65	1000		1354.1	31.3	20.9	1195	0.004	0.048
11	065Ma_1000ppm_orb_22p0-0p00-000	65	1000		1354.1	31.3	20.5	1191	0.007	0.039
12	065Ma_1000ppm_orb_24p5-0p06-090	65	1000		1354.1	31.3	20.9	1195	0.015	0.094
13	065Ma_1000ppm_orb_24p5-0p06-180	65	1000		1354.1	31.3	21.0	1198	0.006	0.025
14	065Ma_1000ppm_orb_24p5-0p06-270	65	1000		1354.1	31.3	20.9	1197	0.012	0.029
15	065Ma_1500ppm	65	1500		1354.1	31.3	22.2	1256	0.009	0.039
16	065Ma_2000ppm	65	2000		1354.1	31.3	23.3	1302	0.012	0.023
17	065Ma_4000ppm	65	4000		1354.1	31.3	25.6	1405	0.016	0.133
18	070Ma_300ppm	70	300	proxy	1353.5	32.2	15.5	983	0.004	-0.001
19	070Ma_800ppm	70	800	COPSE	1353.5	32.2	19.7	1142	0.004	0.036
20	070Ma_1000ppm	70	1000		1353.5	32.2	20.6	1180	0.006	0.037
21	075Ma_250ppm	75	250		1352.9	26.9	15.4	985	0.027	0.003
22	075Ma_500ppm	75	500	proxy	1352.9	26.9	18.4	1096	0.001	0.032
23	075Ma_900ppm	75	900	COPSE	1352.9	26.9	20.8	1193	0.006	0.04
24	075Ma_1000ppm	75	1000		1352.9	26.9	21.2	1211	-0.015	0.054
25	075Ma_1000ppm_S0ini	75	1000		1332.7	26.9	19.5	1130	0.000	0.025
26	075Ma_1000ppm_S0ini_VegFix	75	1000		1332.7	26.9	19.4	1111	-0.010	0.036
27	075Ma_1000ppm_VegHom	75	1000		1352.9	26.9	21.3	1209	0.008	0.055
28	075Ma_1000ppm_orb_22p0-0p00-000	75	1000		1352.9	26.9	21.1	1214	-0.000	0.038
29	075Ma_1000ppm_orb_24p5-0p06-090	75	1000		1352.9	26.9	21.5	1217	0.010	0.064
30	075Ma_1000ppm_orb_24p5-0p06-180	75	1000		1352.9	26.9	21.5	1221	0.001	0.025
31	075Ma_1000ppm_orb_24p5-0p06-270	75	1000		1352.9	26.9	21.4	1221	0.016	0.027
32	075Ma_1500ppm	75	1500		1352.9	26.9	22.7	1276	0.009	0.081
33	075Ma_2000ppm	75	2000		1352.9	26.9	23.7	1321	0.025	0.107
34	075Ma_4000ppm	75	4000		1352.9	26.9	26.0	1422	0.012	0.169
35	080Ma_700ppm	80	700	proxy	1352.4	26.0	19.8	1149	-0.009	0.075
36	080Ma_900ppm	80	900	COPSE	1352.4	26.0	20.8	1192	-0.005	0.036
37	080Ma_1000ppm	80	1000		1352.4	26.0	21.2	1209	0.018	0.02
38	085Ma_600ppm	85	600	proxy	1351.8	27.1	19.1	1122	-0.038	0.019
39	085Ma_900ppm	85	900	COPSE	1351.8	27.1	20.7	1190	0.001	0.036
40	085Ma_1000ppm	85	1000		1351.8	27.1	21.1	1208	0.005	0.041
41	090Ma_500ppm	90	500	proxy	1351.2	28.0	18.1	1086	0.147	0.087
42	090Ma_900ppm	90	900	COPSE	1351.2	28.0	20.5	1185	0.007	0.049
43	090Ma_1000ppm	90	1000		1351.2	28.0	20.9	1203	0.016	0.044
44	095Ma_600ppm	95	600	proxy	1350.6	28.7	18.5	1099	0.004	0.045
45	095Ma_1000ppm	95	1000	COPSE	1350.6	28.7	20.6	1185	-0.001	0.036
46	100Ma_250ppm	100	250		1350.0	30.0	14.4	949	-0.009	0.016
47	100Ma_500ppm	100	500		1350.0	30.0	17.4	1060	-0.016	0.016
48	100Ma_900ppm	100	900	proxy	1350.0	30.0	19.8	1158	0.003	0.072
49	100Ma_1000ppm	100	1000	COPSE	1350.0	30.0	20.2	1176	0.002	0.068
50	100Ma_1000ppm_S0ini	100	1000		1332.7	30.0	18.8	1106	0.000	0.026
51	100Ma_1000ppm_S0ini_VegFix	100	1000		1332.7	30.0	18.7	1098	-0.005	-0.06
52	100Ma_1000ppm_SL+40	100	1000		1350.0	29.7	20.4	1180	0.142	0.031
53	100Ma_1000ppm_SL-200	100	1000		1350.0	37.9	19.1	1120	0.014	0.015
54	100Ma_1000ppm_SL-40	100	1000		1350.0	30.7	20.1	1172	0.005	0.034
55	100Ma_1000ppm_VegHom	100	1000		1350.0	30.0	20.3	1184	0.005	0.068
56	100Ma_1000ppm_VegHom_SL+40	100	1000		1350.0	29.7	20.5	1188	0.074	0.046
57	100Ma_1000ppm_VegHom_SL-200	100	1000		1350.0	37.9	19.1	1124	-0.013	0.059
58	100Ma_1000ppm_VegHom_SL-40	100	1000		1350.0	30.7	20.2	1180	0.000	0.01
59	100Ma_1000ppm_orb_22p0-0p00-000	100	1000		1350.0	30.0	20.1	1178	0.005	0.067
60	100Ma_1000ppm_orb_24p5-0p06-090	100	1000		1350.0	30.0	20.5	1187	0.007	0.043
61	100Ma_1000ppm_orb_24p5-0p06-180	100	1000		1350.0	30.0	20.5	1185	0.011	0.051
62	100Ma_1000ppm_orb_24p5-0p06-270	100	1000		1350.0	30.0	20.5	1183	0.007	0.045
63	100Ma_1500ppm	100	1500		1350.0	30.0	21.8	1243	0.025	0.081
64	100Ma_2000ppm	100	2000		1350.0	30.0	22.8	1289	0.017	0.114
65	100Ma_4000ppm	100	4000		1350.0	30.0	25.1	1394	0.011	0.158
66	105Ma_1000ppm	105	1000	proxy	1349.5	30.5	20.3	1178	0.005	0.081
67	105Ma_1100ppm	105	1100	COPSE	1349.5	30.5	20.7	1195	-0.001	0.077
68	110Ma_1000ppm	110	1000		1348.9	30.6	20.3	1161	0.001	0.035
69	110Ma_1100ppm	110	1100	proxyCOPSE	1348.9	30.6	20.7	1177	0.002	0.027
70	115Ma_1000ppm	115	1000	COPSE	1348.3	30.3	20.2	1152	0.002	0.052
71	115Ma_1100ppm	115	1100	proxy	1348.3	30.3	20.6	1169	0.003	0.053
72	120Ma_1000ppm	120	1000	proxyCOPSE	1347.7	30.4	19.8	1128	-0.000	0.058
73	125Ma_250ppm	125	250		1347.2	31.1	13.5	900	-0.003	0.033
74	125Ma_500ppm	125	500		1347.2	31.1	16.9	1014	-0.000	0.027
75	125Ma_900ppm	125	900	proxy	1347.2	31.1	19.5	1116	0.001	0.034
76	125Ma_1000ppm	125	1000	COPSE	1347.2	31.1	19.9	1135	0.003	0.039
77	125Ma_1000ppm_S0ini	125	1000		1332.7	31.1	18.6	1074	0.000	0.032
78	125Ma_1000ppm_S0ini_VegFix	125	1000		1332.7	31.1	18.8	1090	0.001	0.042
79	125Ma_1000ppm_VegHom	125	1000		1347.2	31.1	20.1	1152	0.003	0.048
80	125Ma_1000ppm_orb_22p0-0p00-000	125	1000		1347.2	31.1	19.8	1135	0.002	0.035
81	125Ma_1000ppm_orb_24p5-0p06-090	125	1000		1347.2	31.1	20.2	1146	0.003	0.008
82	125Ma_1000ppm_orb_24p5-0p06-180	125	1000		1347.2	31.1	20.2	1149	0.003	0.026
83	125Ma_1000ppm_orb_24p5-0p06-270	125	1000		1347.2	31.1	20.1	1147	0.003	0.015
84	125Ma_1500ppm	125	1500		1347.2	31.1	21.5	1206	0.006	0.062
85	125Ma_2000ppm	125	2000		1347.2	31.1	22.6	1255	0.009	0.083
86	125Ma_4000ppm	125	4000		1347.2	31.1	24.9	1367	0.021	0.136
87	130Ma_900ppm	130	900	proxyCOPSE	1346.6	33.5	19.1	1092	-0.015	0.023
88	130Ma_1000ppm	130	1000		1346.6	33.5	19.5	1111	-0.004	0.022
89	135Ma_1000ppm	135	1000	proxyCOPSE	1346.0	34.2	19.3	1103	0.002	0.017
90	140Ma_900ppm	140	900	proxyCOPSE	1345.4	34.9	18.6	1077	-0.001	0.01

91	140Ma_1000ppm	140	1000		1345.4	34.9	19.0	1096	-0.001	0.023
92	145Ma_700ppm	145	700	proxyCOPSE	1344.8	34.3	17.5	1027	-0.013	0.022
93	145Ma_1000ppm	145	1000		1344.8	34.3	19.1	1093	-0.000	0.02
94	150Ma_250ppm	150	250		1344.3	34.2	12.0	825	-0.003	0.004
95	150Ma_500ppm	150	500		1344.3	34.2	15.7	946	-0.005	-0.01
96	150Ma_700ppm	150	700	COPSE	1344.3	34.2	17.3	1007	-0.035	0.027
97	150Ma_800ppm	150	800	proxy	1344.3	34.2	18.0	1032	-0.009	0.023
98	150Ma_1000ppm	150	1000		1344.3	34.2	18.9	1072	-0.004	0.034
99	150Ma_1000ppm_S0ini	150	1000		1332.7	34.2	17.9	1023	-0.023	0.038
100	150Ma_1000ppm_S0ini_VegFix	150	1000		1332.7	34.2	18.3	1066	0.003	0.012
101	150Ma_1000ppm_SL+40	150	1000		1344.3	33.6	19.1	1074	-0.001	0.025
102	150Ma_1000ppm_SL-40	150	1000		1344.3	36.5	18.6	1050	0.005	0.029
103	150Ma_1000ppm_VegHom	150	1000		1344.3	34.2	19.3	1110	0.001	0.016
104	150Ma_1000ppm_VegHom_SL+40	150	1000		1344.3	33.6	19.5	1114	-0.000	0.015
105	150Ma_1000ppm_VegHom_SL-40	150	1000		1344.3	36.5	18.9	1087	-0.007	0.022
106	150Ma_1000ppm_orb_22p0-0p00-000	150	1000		1344.3	34.2	18.8	1071	-0.003	0.031
107	150Ma_1000ppm_orb_24p5-0p06-090	150	1000		1344.3	34.2	19.2	1084	0.001	0.024
108	150Ma_1000ppm_orb_24p5-0p06-180	150	1000		1344.3	34.2	19.2	1086	0.001	0.007
109	150Ma_1000ppm_orb_24p5-0p06-270	150	1000		1344.3	34.2	19.2	1084	0.004	0.016
110	150Ma_1500ppm	150	1500		1344.3	34.2	20.6	1143	0.002	0.046
111	150Ma_2000ppm	150	2000		1344.3	34.2	21.7	1193	0.010	0.074
112	150Ma_4000ppm	150	4000		1344.3	34.2	24.2	1309	0.016	0.093
113	155Ma_700ppm	155	700	COPSE	1343.7	31.9	17.7	1018	0.057	0.043
114	155Ma_800ppm	155	800	proxy	1343.7	31.9	18.3	1043	0.153	0.007
115	155Ma_1000ppm	155	1000		1343.7	31.9	19.3	1083	-0.002	0.02
116	160Ma_600ppm	160	600	COPSE	1343.1	28.2	17.3	1005	0.000	0.025
117	160Ma_800ppm	160	800	proxy	1343.1	28.2	18.7	1059	0.001	0.032
118	160Ma_1000ppm	160	1000		1343.1	28.2	19.7	1101	0.000	0.034
119	165Ma_600ppm	165	600	COPSE	1342.5	30.5	16.8	978	0.007	0.027
120	165Ma_900ppm	165	900	proxy	1342.5	30.5	18.8	1059	0.157	-0.029
121	165Ma_1000ppm	165	1000		1342.5	30.5	19.3	1078	0.000	0.007
122	170Ma_500ppm	170	500	COPSE	1341.9	32.5	15.4	919	-0.005	0.021
123	170Ma_1000ppm	170	1000	proxy	1341.9	32.5	19.0	1053	-0.000	0.023
124	175Ma_250ppm	175	250		1341.4	33.6	10.9	785	0.000	0.042
125	175Ma_500ppm	175	500	COPSE	1341.4	33.6	15.0	914	0.001	0.024
126	175Ma_1000ppm	175	1000	proxy	1341.4	33.6	18.7	1051	-0.001	0.027
127	175Ma_1000ppm_S0ini	175	1000		1332.7	33.6	17.8	1012	0.027	0.035
128	175Ma_1000ppm_S0ini_VegFix	175	1000		1332.7	33.6	18.3	1065	0.001	0.012
129	175Ma_1000ppm_VegHom	175	1000		1341.4	33.6	19.0	1097	0.000	0.016
130	175Ma_1000ppm_orb_22p0-0p00-000	175	1000		1341.4	33.6	18.6	1050	0.004	0.009
131	175Ma_1000ppm_orb_24p5-0p06-090	175	1000		1341.4	33.6	18.9	1060	-0.000	0.015
132	175Ma_1000ppm_orb_24p5-0p06-180	175	1000		1341.4	33.6	19.0	1067	-0.001	0.002
133	175Ma_1000ppm_orb_24p5-0p06-270	175	1000		1341.4	33.6	19.0	1070	-0.000	-0.008
134	175Ma_1500ppm	175	1500		1341.4	33.6	20.4	1127	0.002	0.014
135	175Ma_2000ppm	175	2000		1341.4	33.6	21.6	1180	-0.005	0.006
136	175Ma_4000ppm	175	4000		1341.4	33.6	24.1	1305	-0.000	0.018
137	180Ma_500ppm	180	500	COPSE	1340.9	38.2	14.1	865	-0.009	0.017
138	180Ma_900ppm	180	900	proxy	1340.9	38.2	17.4	980	-0.007	0.001
139	180Ma_1000ppm	180	1000		1340.9	38.2	17.9	1000	0.005	0.015
140	185Ma_500ppm	185	500	COPSE	1340.3	35.8	14.5	887	0.091	-0.005
141	185Ma_900ppm	185	900	proxy	1340.3	35.8	17.8	1005	-0.002	0.006
142	185Ma_1000ppm	185	1000		1340.3	35.8	18.3	1026	0.018	0.005
143	190Ma_500ppm	190	500	COPSE	1339.8	35.1	14.8	886	0.001	0.023
144	190Ma_1000ppm	190	1000		1339.8	35.1	18.5	1016	-0.000	0.038
145	190Ma_1100ppm	190	1100	proxy	1339.8	35.1	18.9	1033	-0.000	0.033
146	195Ma_500ppm	195	500	COPSE	1339.2	35.1	14.2	864	0.000	0.029
147	195Ma_1000ppm	195	1000		1339.2	35.1	18.1	1001	-0.016	0.005
148	195Ma_1700ppm	195	1700	proxy	1339.2	35.1	20.5	1098	-0.114	0.059
149	200Ma_250ppm	200	250		1338.7	37.4	9.9	731	0.002	0.031
150	200Ma_500ppm	200	500	COPSE	1338.7	37.4	13.9	847	-0.010	0.028
151	200Ma_1000ppm	200	1000		1338.7	37.4	17.8	978	0.006	0.027
152	200Ma_1000ppm_S0ini	200	1000		1332.7	37.4	17.2	952	0.001	0.02
153	200Ma_1000ppm_S0ini_VegFix	200	1000		1332.7	37.4	17.6	1003	-0.009	0.016
154	200Ma_1000ppm_SL+200	200	1000		1338.7	32.0	19.0	1011	-0.009	0.013
155	200Ma_1000ppm_SL+40	200	1000		1338.7	36.0	18.1	990	-0.017	0.016
156	200Ma_1000ppm_VegHom	200	1000		1338.7	37.4	18.2	1030	0.006	0.014
157	200Ma_1000ppm_VegHom_SL+200	200	1000		1338.7	32.0	19.3	1060	-0.043	0.078
158	200Ma_1000ppm_VegHom_SL+40	200	1000		1338.7	36.0	18.5	1042	-0.147	0.009
159	200Ma_1000ppm_orb_22p0-0p00-000	200	1000		1338.7	37.4	17.7	972	0.007	0.038
160	200Ma_1000ppm_orb_24p5-0p06-090	200	1000		1338.7	37.4	18.1	997	0.021	0.001
161	200Ma_1000ppm_orb_24p5-0p06-180	200	1000		1338.7	37.4	18.1	996	0.002	-0.009
162	200Ma_1000ppm_orb_24p5-0p06-270	200	1000		1338.7	37.4	18.1	995	0.033	-0.013
163	200Ma_1500ppm	200	1500		1338.7	37.4	19.7	1052	-0.006	0.015
164	200Ma_1700ppm	200	1700	proxy	1338.7	37.4	20.2	1074	0.019	0.023
165	200Ma_2000ppm	200	2000		1338.7	37.4	20.9	1102	0.005	0.024
166	200Ma_4000ppm	200	4000		1338.7	37.4	23.4	1223	-0.017	0.044
167	205Ma_600ppm	205	600	COPSE	1338.1	37.1	15.0	873	0.001	0.034
168	205Ma_1000ppm	205	1000		1338.1	37.1	17.8	971	0.005	0.016
169	205Ma_1500ppm	205	1500	proxy	1338.1	37.1	19.6	1045	0.008	0.035
170	210Ma_800ppm	210	800	COPSE	1337.6	36.6	16.6	925	0.043	0.051
171	210Ma_1000ppm	210	1000		1337.6	36.6	17.7	967	-0.005	0.019
172	210Ma_1300ppm	210	1300	proxy	1337.6	36.6	19.0	1017	-0.034	0.004
173	215Ma_900ppm	215	900	COPSE	1337.0	36.9	17.4	962	0.001	0.032
174	215Ma_1000ppm	215	1000		1337.0	36.9	17.9	982	0.000	0.018
175	215Ma_1300ppm	215	1300	proxy	1337.0	36.9	19.2	1032	0.000	0.011
176	220Ma_1000ppm	220	1000	COPSE	1336.5	30.6	18.2	1011	0.009	0.004
177	220Ma_1600ppm	220	1600	proxy	1336.5	30.6	20.4	1101	-0.005	0.013
178	225Ma_250ppm	225	250		1336.0	30.9	9.1	719	0.001	0.047
179	225Ma_500ppm	225	500		1336.0	30.9	13.8	844	-0.000	0.06
180	225Ma_900ppm	225	900	COPSE	1336.0	30.9	17.3	962	0.000	-0.005
181	225Ma_1000ppm	225	1000		1336.0	30.9	17.9	983	0.001	0.003
182	225Ma_1000ppm_S0ini	225	1000		1332.7	30.9	17.5	968	0.000	0
183	225Ma_1000ppm_S0ini_VegFix	225	1000		1332.7	30.9	18.4	1052	0.000	-0.021
184	225Ma_1000ppm_VegHom	225	1000		1336.0	30.9	18.3	1032	0.000	-0.013
185	225Ma_1000ppm_orb_22p0-0p00-000	225	1000		1336.0	30.9	17.7	981	0.000	0.005
186	225Ma_1000ppm_orb_24p5-0p06-090	225	1000		1336.0	30.9	18.3	1003	-0.000	0.005
187	225Ma_1000ppm_orb_24p5-0p06-180	225	1000		1336.0	30.9	18.2	997	0.002	0.004
188	225Ma_1000ppm_orb_24p5-0p06-270	225	1000		1336.0	30.9	18.3	993	-0.004	-0.025
189	225Ma_1500ppm	225	1500		1336.0	30.9	19.9	1059	-0.006	0.002
190	225Ma_2000ppm	225	2000	proxy	1336.0	30.9	21.1	1111	-0.022	0.008
191	225Ma_4000ppm	225	4000		1336.0	30.9	23.6	1227	0.001	0.016
192	230Ma_800ppm	230	800	COPSE	1335.4	31.6	16.5	936	0.001	0.008
193	230Ma_1000ppm	230	1000		1335.4	31.6	17.7	979	0.009	-0.004

194	230Ma_1900ppm	230	1900	proxy	1335.4	31.6	20.7	1099	-0.000	0.001
195	235Ma_800ppm	235	800	COPSE	1334.9	32.0	16.6	934	0.010	0.038
196	235Ma_1000ppm	235	1000		1334.9	32.0	17.9	979	0.003	-0.004
197	235Ma_1400ppm	235	1400	proxy	1334.9	32.0	19.4	1040	-0.003	-0
198	240Ma_800ppm	240	800	proxy	1334.3	31.7	16.5	942	0.026	0.008
199	240Ma_900ppm	240	900	COPSE	1334.3	31.7	17.2	964	0.041	0.022
200	240Ma_1000ppm	240	1000		1334.3	31.7	17.8	984	0.004	0.016
201	245Ma_400ppm	245	400	proxy	1333.8	31.3	12.9	818	-0.001	0.049
202	245Ma_1000ppm	245	1000	COPSE	1333.8	31.3	18.1	992	0.001	-0.015
203	250Ma_250ppm	250	250		1333.2	30.8	10.3	740	0.001	0.016
204	250Ma_500ppm	250	500		1333.2	30.8	14.9	869	-0.001	0.022
205	250Ma_700ppm	250	700	proxy	1333.2	30.8	16.8	933	0.000	0.005
206	250Ma_1000ppm	250	1000		1333.2	30.8	18.5	998	0.001	-0.009
207	250Ma_1000ppm_S0ini	250	1000		1332.7	30.8	18.5	996	-0.011	-0.01
208	250Ma_1000ppm_S0ini_VegFix	250	1000		1332.7	30.8	18.8	1040	-0.003	-0.009
209	250Ma_1000ppm_VegHom	250	1000		1333.2	30.8	18.8	1039	-0.003	-0.005
210	250Ma_1000ppm_orb_22p0-0p00-000	250	1000		1333.2	30.8	18.4	995	-0.005	-0.005
211	250Ma_1000ppm_orb_24p5-0p06-090	250	1000		1333.2	30.8	18.7	1023	-0.048	0.021
212	250Ma_1000ppm_orb_24p5-0p06-180	250	1000		1333.2	30.8	18.8	1016	-0.012	0.008
213	250Ma_1000ppm_orb_24p5-0p06-270	250	1000		1333.2	30.8	18.9	1008	0.014	0.005
214	250Ma_1100ppm	250	1100	COPSE	1333.2	30.8	18.9	1015	0.003	-0.011
215	250Ma_1500ppm	250	1500		1333.2	30.8	20.3	1070	-0.001	-0.02
216	250Ma_2000ppm	250	2000		1333.2	30.8	21.4	1120	0.009	-0.011
217	250Ma_4000ppm	250	4000		1333.2	30.8	23.9	1238	0.002	-0.011
218	255Ma_800ppm	255	800	proxy	1332.7	29.6	17.6	967	-0.001	-0.004
219	255Ma_1000ppm	255	1000		1332.7	29.6	18.6	1007	0.002	-0
220	255Ma_1300ppm	255	1300	COPSE	1332.7	29.6	19.8	1054	0.002	0.016

References

Boucot, A. J., Xu, C., Scotese, C. R., & Morley, R. J. (2013). *Phanerozoic Paleoclimate: An Atlas of Lithologic Indicators of Climate*. SEPM Society for Sedimentary Geology. doi: 10.2110/sepmcsp.11

Cao, W., Williams, S., Flament, N., Zahirovic, S., Scotese, C. R., & Müller, R. D. (2018). Palaeolatitudinal distribution of lithologic indicators of climate in a palaeogeographic framework. *Geological Magazine*, *156*(2), 331-354. doi: 10.1017/S0016756818000110

Farnsworth, A., Lunt, D. J., O'Brien, C. L., Foster, G. L., Inglis, G. N., Markwick, P., ... Robinson, S. A. (2019a). Climate Sensitivity on Geological Timescales Controlled by Nonlinear Feedbacks and Ocean Circulation. *Geophysical Research Letters*, *46*. doi: 10.1029/2019GL083574

Laugié, M., Donnadieu, Y., Ladant, J.-B., Green, J. A. M., Bopp, L., & Raisson, F. (2020). Stripping back the modern to reveal the Cenomanian–Turonian climate and temperature gradient underneath. *Climate of the Past*, *16*(3), 953–971. doi: 10.5194/cp-16-953-2020

Mills, B. J., Krause, A. J., Scotese, C. R., Hill, D. J., Shields, G. A., & Lenton, T. M. (2019). Modelling the long-term carbon cycle, atmospheric CO2, and Earth surface temperature from late Neoproterozoic to present day. *Gondwana Research*, *67*, 172 - 186. doi: 10.1016/j.gr.2018.12.001

Scotese, C. R. (2008). The PALEOMAP Project PaleoAtlas for ArcGIS, Volume 2, Cretaceous paleogeographic and plate tectonic reconstructions. *PALEOMAP Project, Arlington, Texas*.

Scotese, C. R. (2016). *Global Climate Change (Modern Times to 540 million years ago).* Retrieved from https://www.researchgate.net/publication/303811641_Global_Climate_Change_Modern_Times_to_540_million_years_ago

Scotese, C. R., & Wright, N. (2018). PALEOMAP paleodigital elevation models (PaleoDEMS) for the Phanerozoic. Retrieved from https://www.earthbyte.org/paleodem-resource-scotese-and-wright-2018

Steinig, S., Dummann, W., Park, W., Latif, M., Kusch, S., Hofmann, P., & Flögel, S. (2020). Evidence for a regional warm bias in the Early Cretaceous TEX86 record. *Earth and Planetary Science Letters*, *539*, 116184. doi: 10.1016/j.epsl.2020.116184

Valdes, P. J., Scotese, C. R., & Lunt, D. J. (2020). Deep Ocean Temperatures through Time. *Climate of the Past Discussions*, 1–37. doi: 10.5194/cp-2020-83

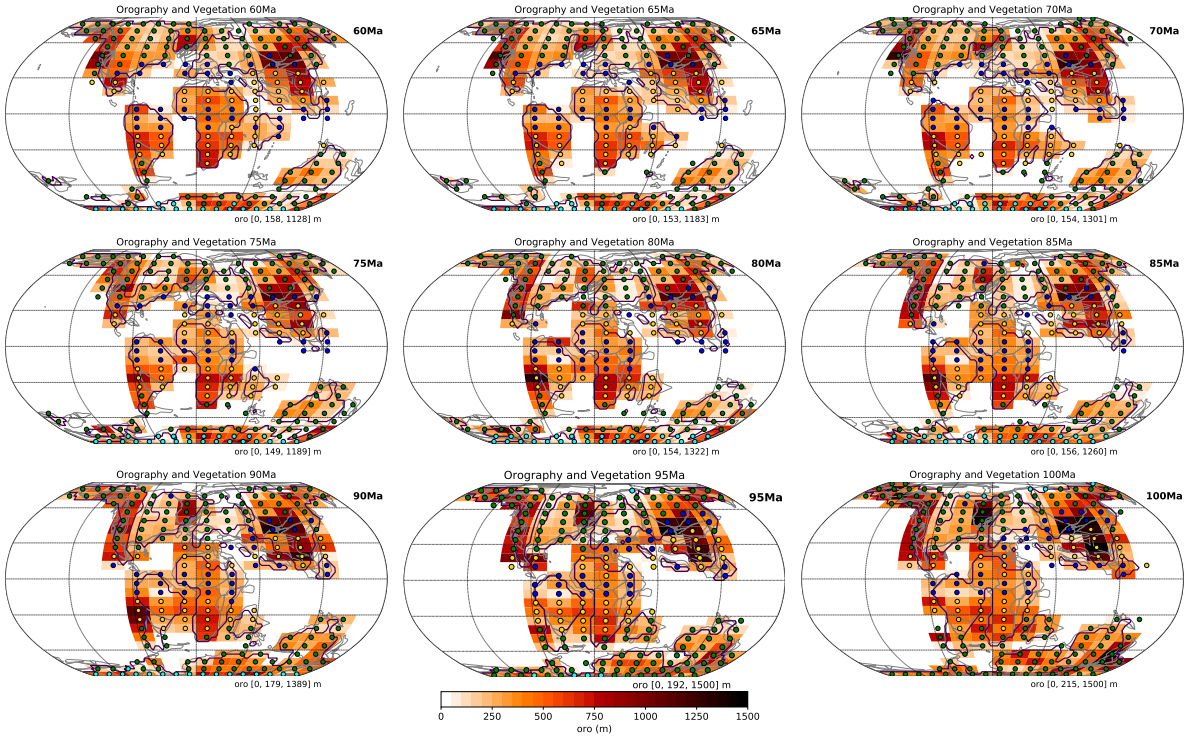

Figure S1. Orography (colors, based on Scotese and Wright (2018)) and Vegetation cover (dots) on the atmosphere model grid for all timeslices. The black lines indicate the land-sea mask on the ocean model grid resolution. Dots indicate the vegetation patterns (`VegHet`) approximated from the proxy-inferred climate zones from (Boucot et al., 2013; Scotese, 2016). Blue: tropical/boreotropical (75 % tree, 20 % grass/shrub, 5 % bare soil), yellow: arid (15 %, 35 %, 60 %), green: warm temperate (70 %, 20 %, 10 %), cyan: cold temperate (65 %, 15 %, 20 %), grey: polar (10 %, 25 %, 65 %)

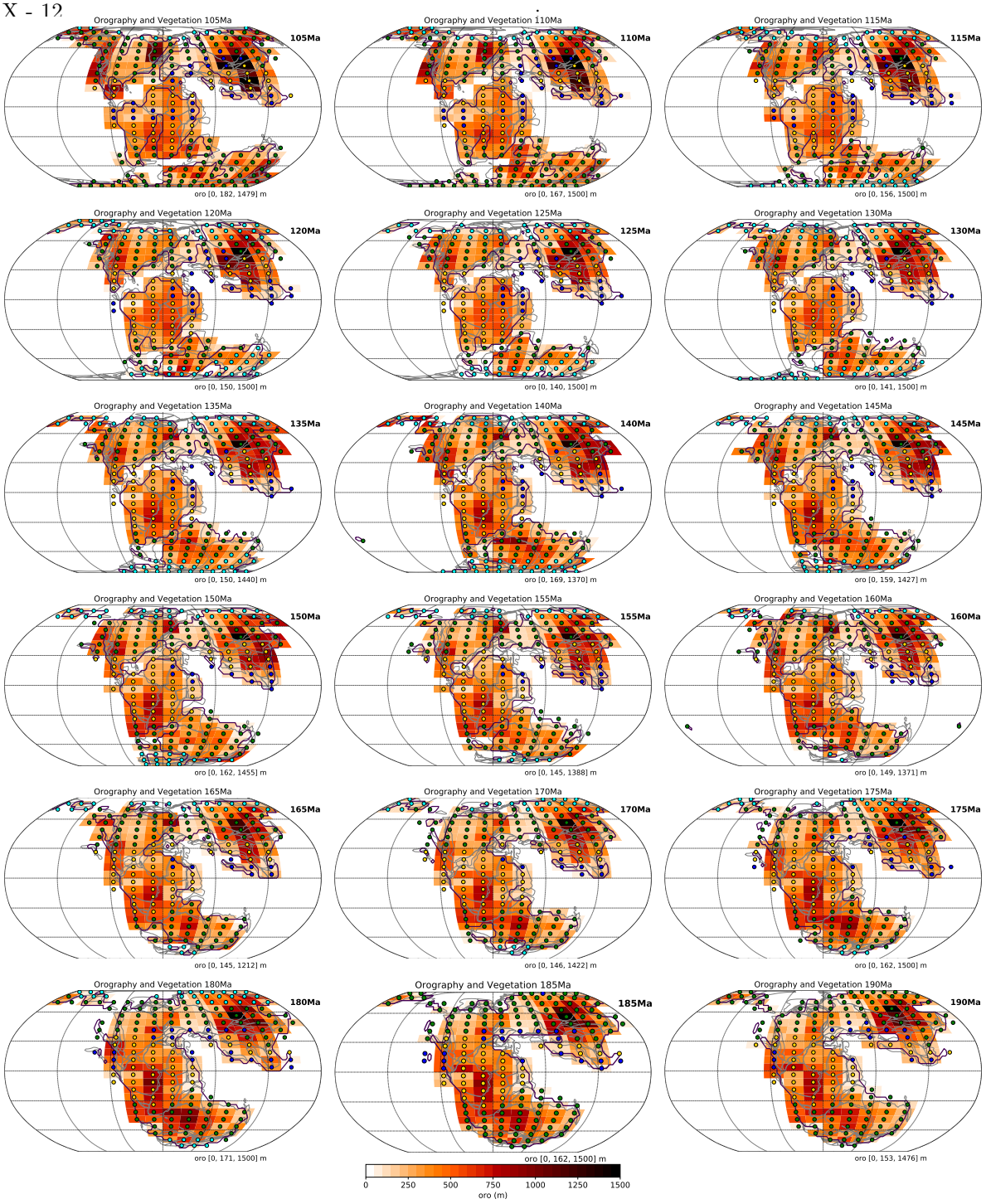

... Fig. S1 continued

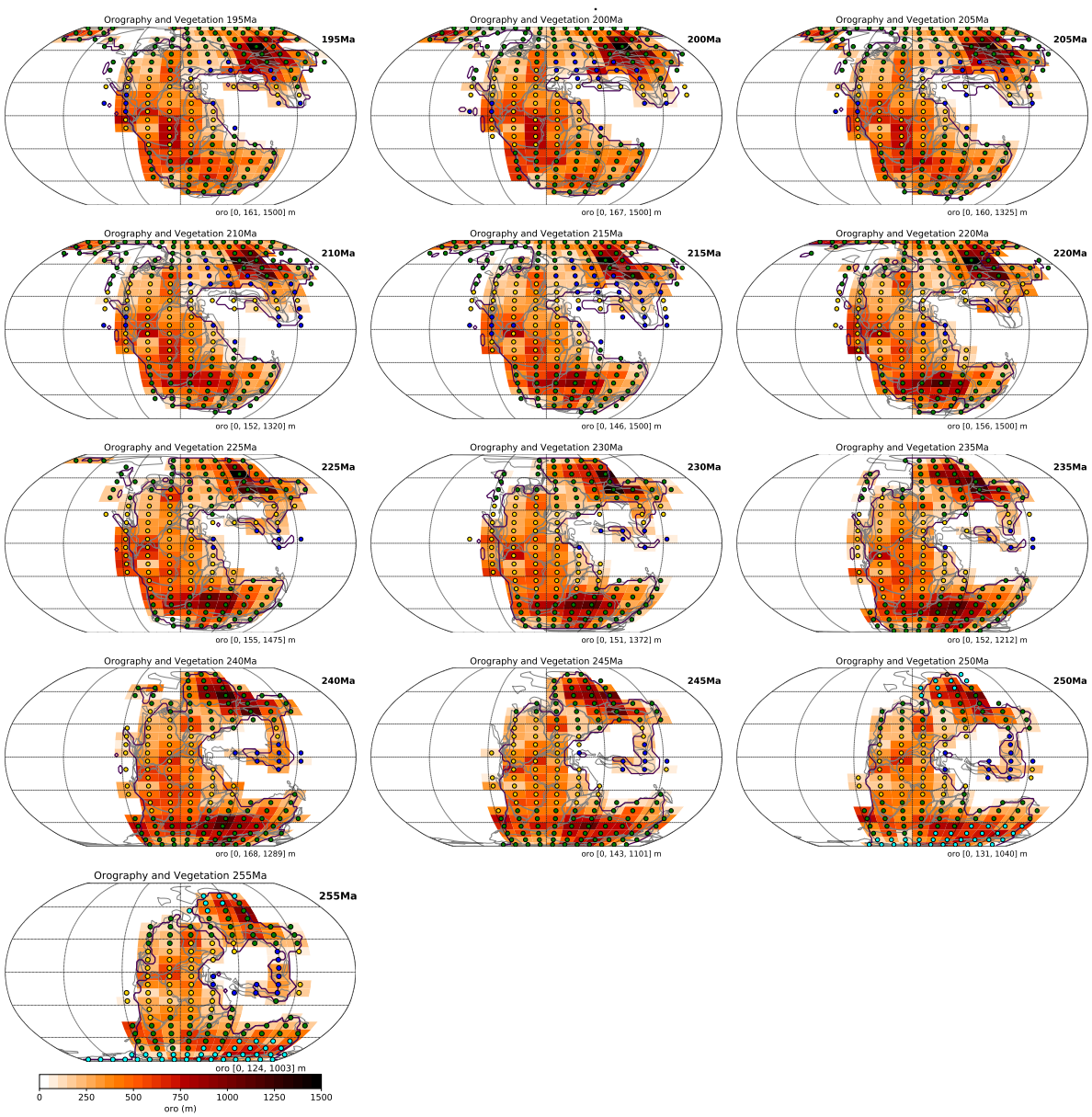

... Fig. S1 continued

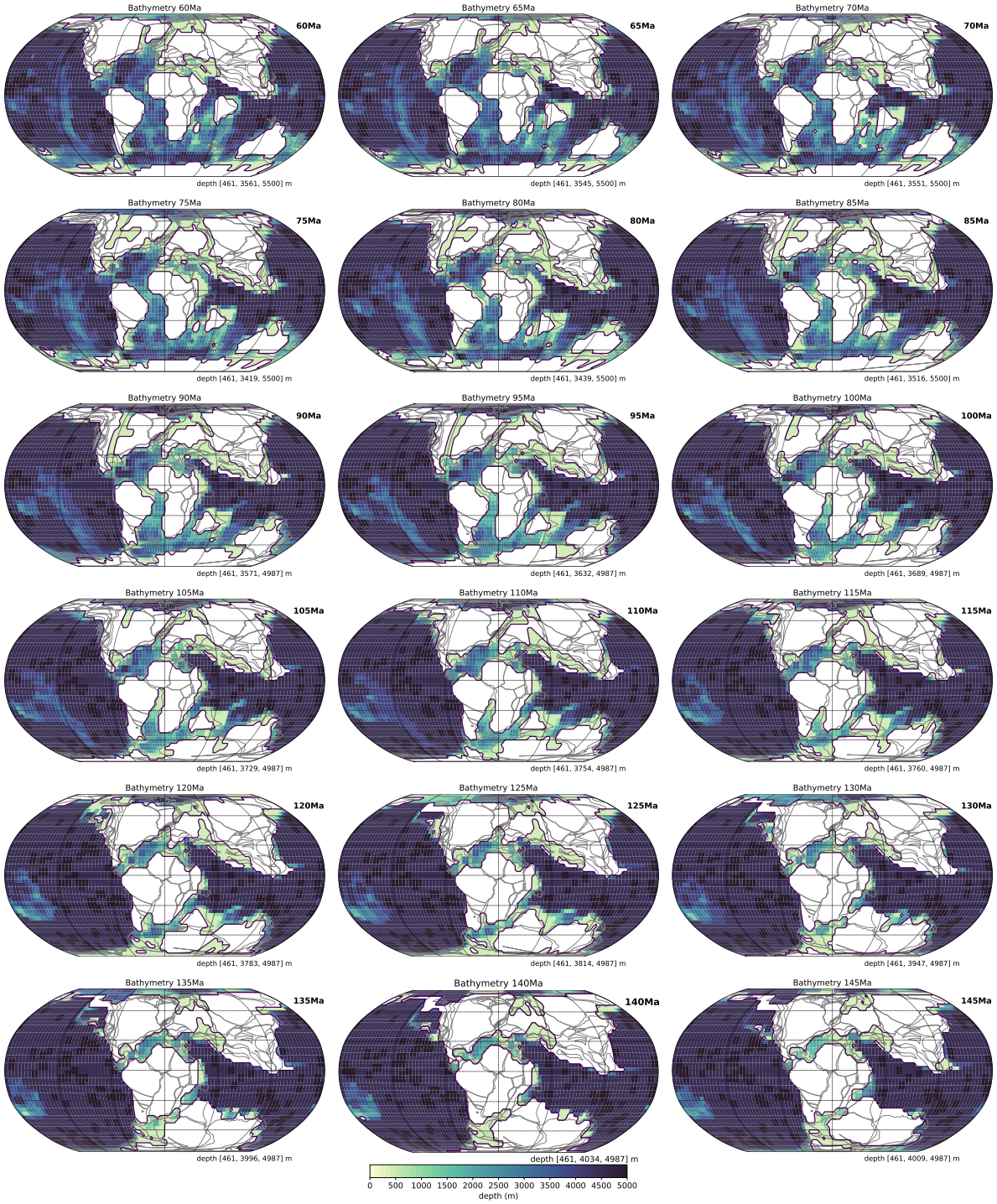

Figure S2. Bathymetry for all timeslices as implemented in the simulations based on Scotese and Wright (2018). Adjustments were made due to model requirements (see Supp. Sec. 1 for further explanation).

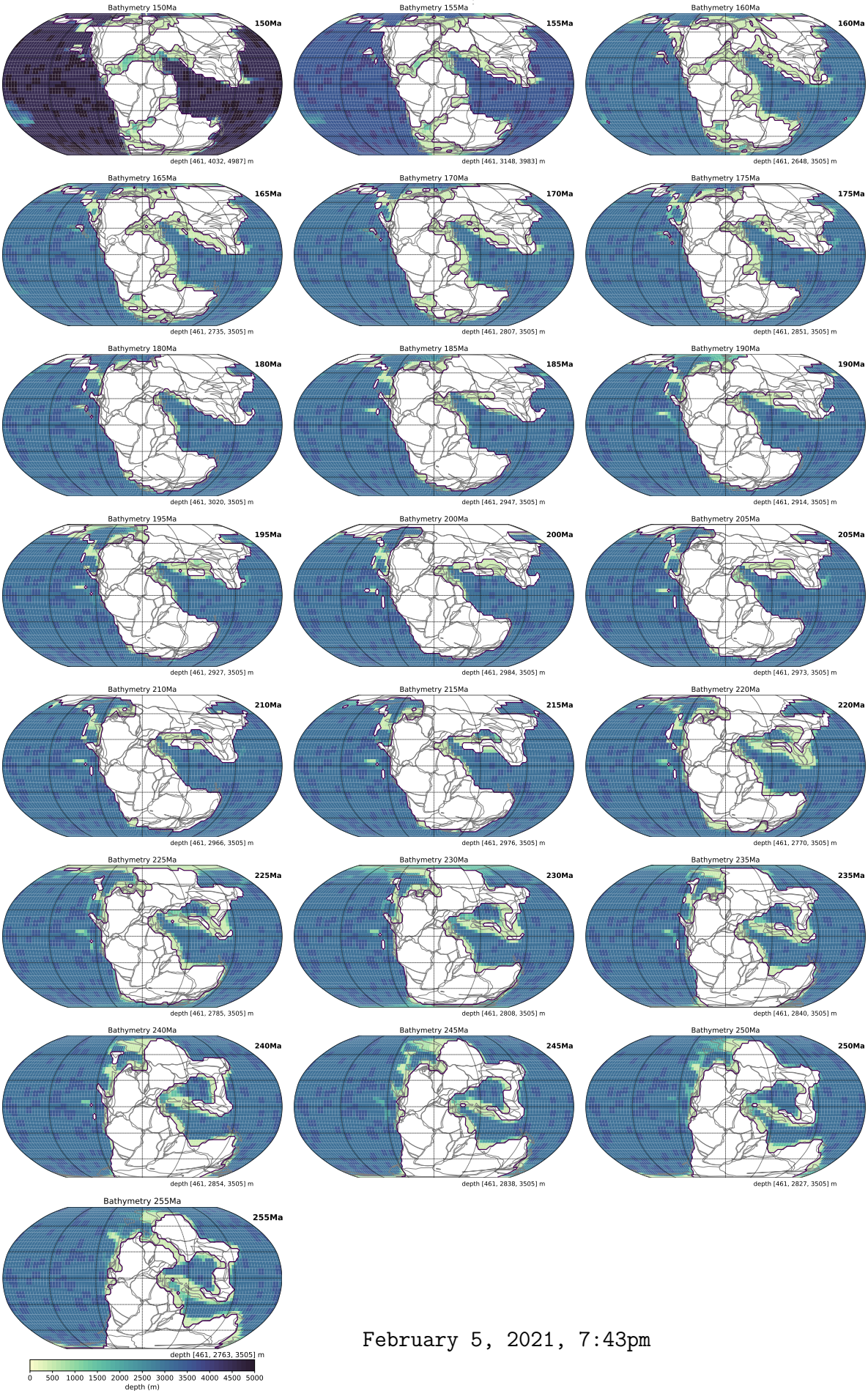

February 5, 2021, 7:43pm

... Fig. S2 continued

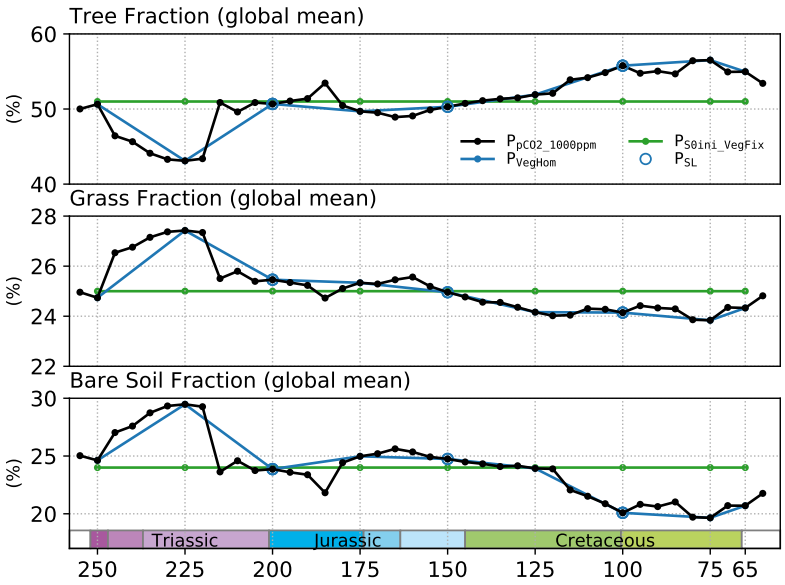

Figure S3. Global mean fractions of tree, grass/shrub and bare soil land cover fraction in different boundary condition pathways.

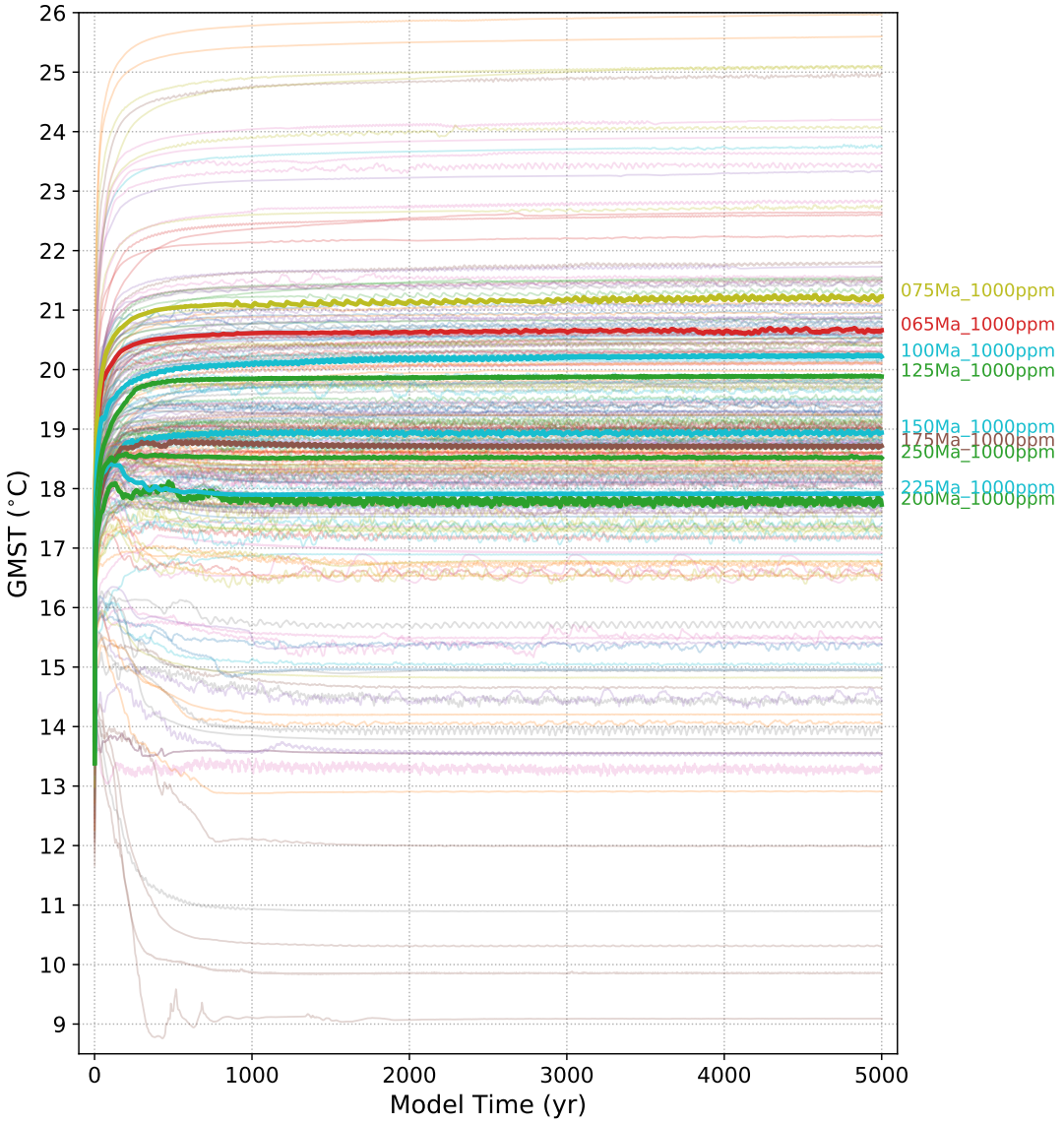

Figure S4. Global mean surface air temperature (GMST) during spin-up for all simulation runs. For the highlighted representative subset of runs ($\mathtt{P}_{\mathtt{pCO2\_1000ppm}}$ for $\mathtt{T}_{\mathtt{25Myr}}$), mean ocean temperatures and salinity timeseries are shown in Fig. S21.

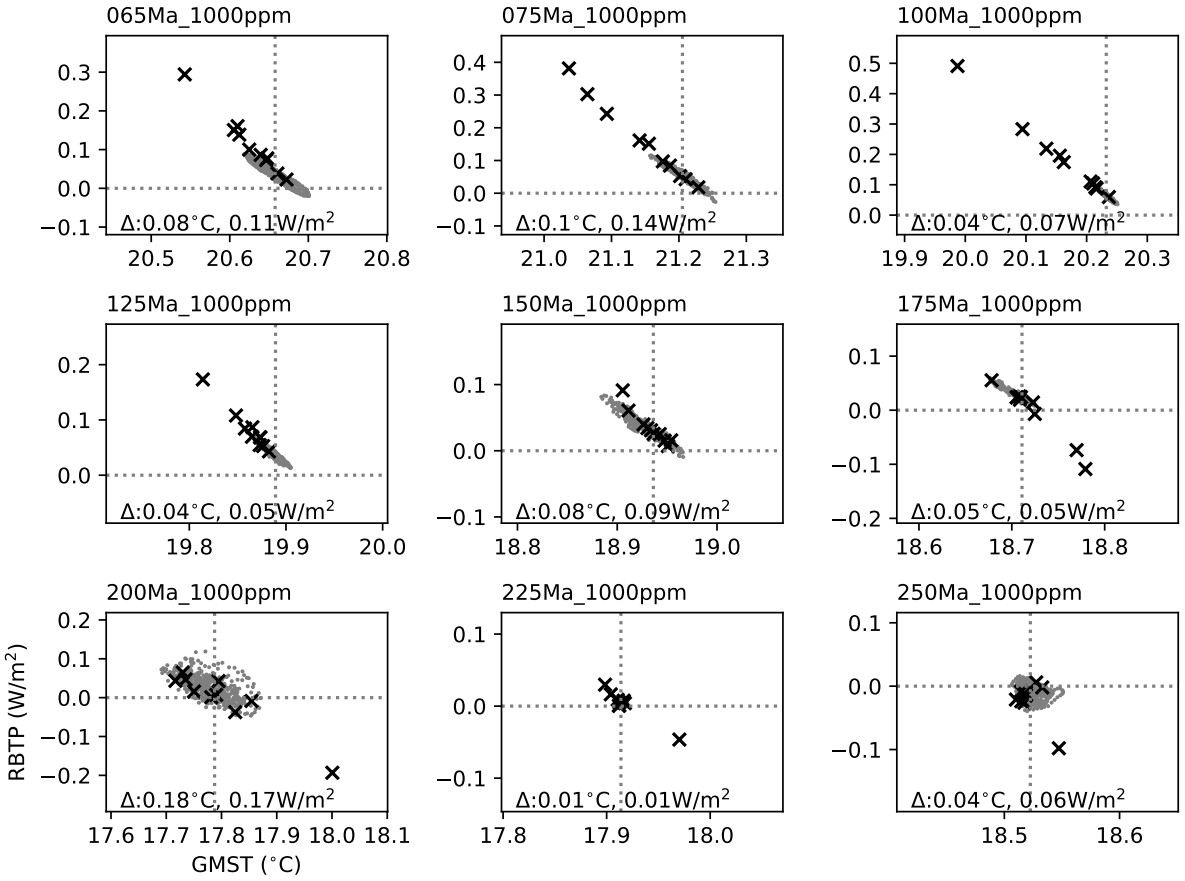

Figure S5. Global mean top-of-the-atmosphere radiation balance (RBTP) over the global mean surface air temperature (GMST) during spinup (Gregory Plot), for the $\mathtt{T}_{\mathtt{25Myr}}$ timeslices of the $\mathtt{P}_{\mathtt{pCO2\_1000ppm}}$ pathway. Crosses represent 500 yr timesteps from model year 500 to 5000, while grey dots represent annual data over the last 500 years of the simulations (years 4500–5000). The maximum variation of GMST and RBTP over the last 500 years is also given in each panel. The vertical dashed line indicates the average GMST over the last 500 years.

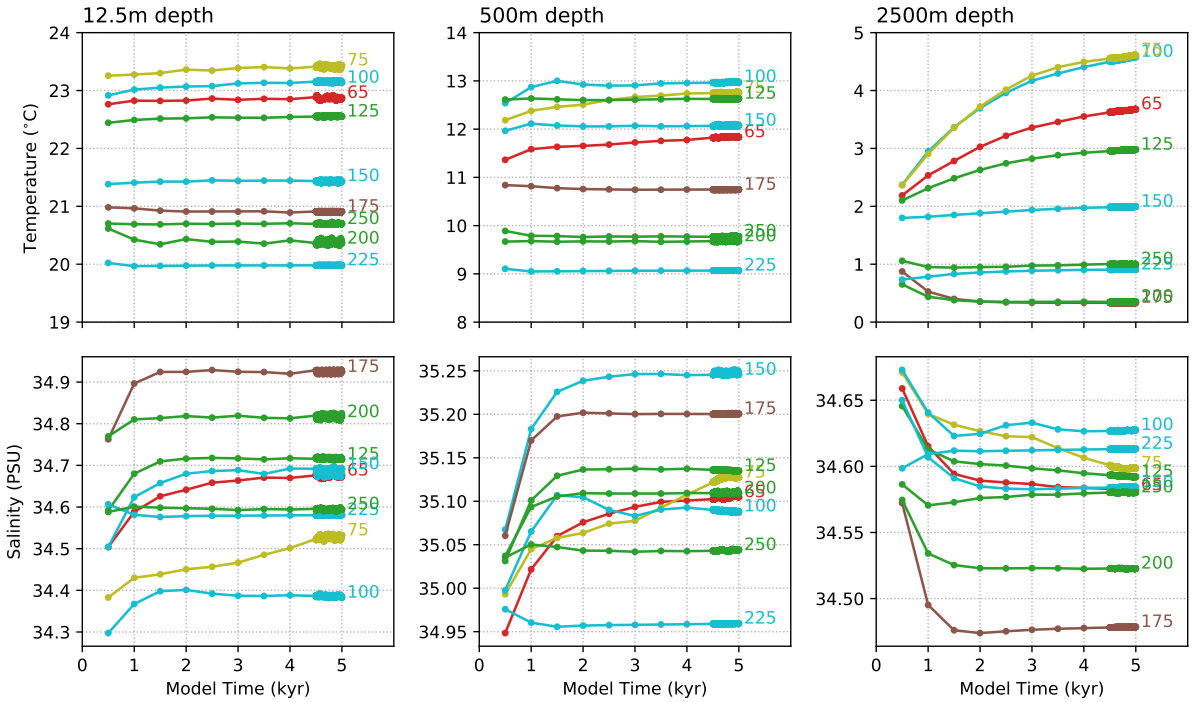

Figure S6. Global mean seawater temperature and salinity at three depth levels during spinup for a subset of the simulation runs ($\mathtt{P}_{\mathtt{pCO2\_1000ppm}}$ for $\mathtt{T}_{\mathtt{25Myr}}$, also see Figs. S4,S5).

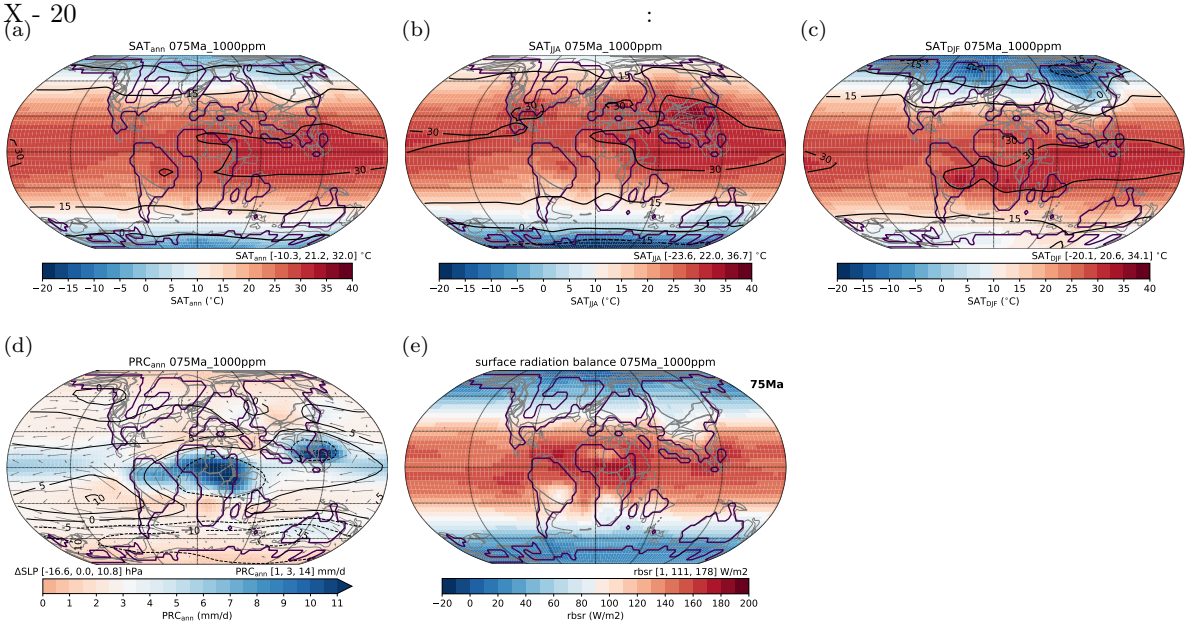

Figure S7. Annual mean surface air temperatures (a), precipitation rates (d) and surface radiation balance (e) for the $\mathtt{P_{pCO2\_1000ppm}}$ pathway at 75 Ma. Seasonal JJA and DJF surface air temperatures (b,c) for the same simulation. Similar plots are included in the accompanying data repository for all runs (AllRuns_Maps.pdf)

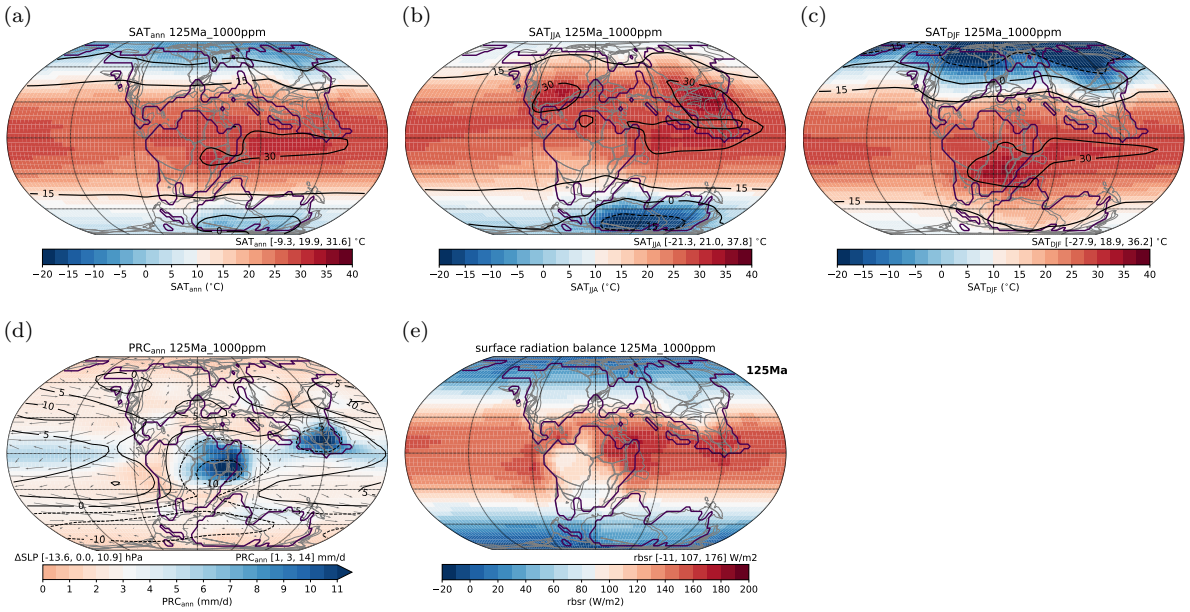

Figure S8. Same as Fig. S7 but at 125 Ma

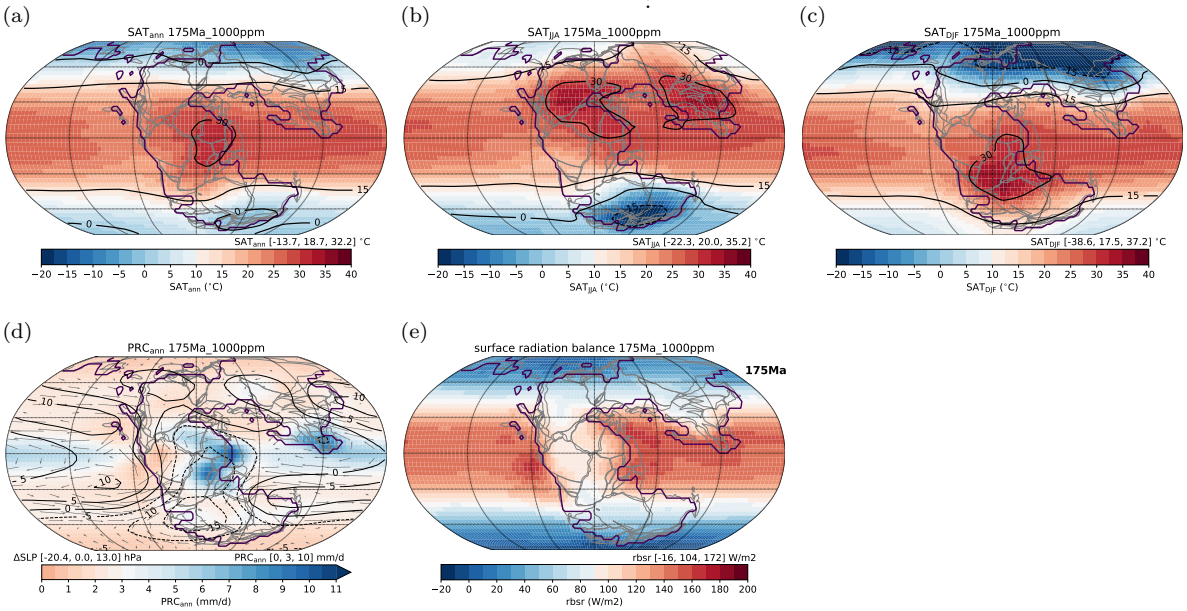

Figure S9. Same as Fig. S7 but at 175 Ma

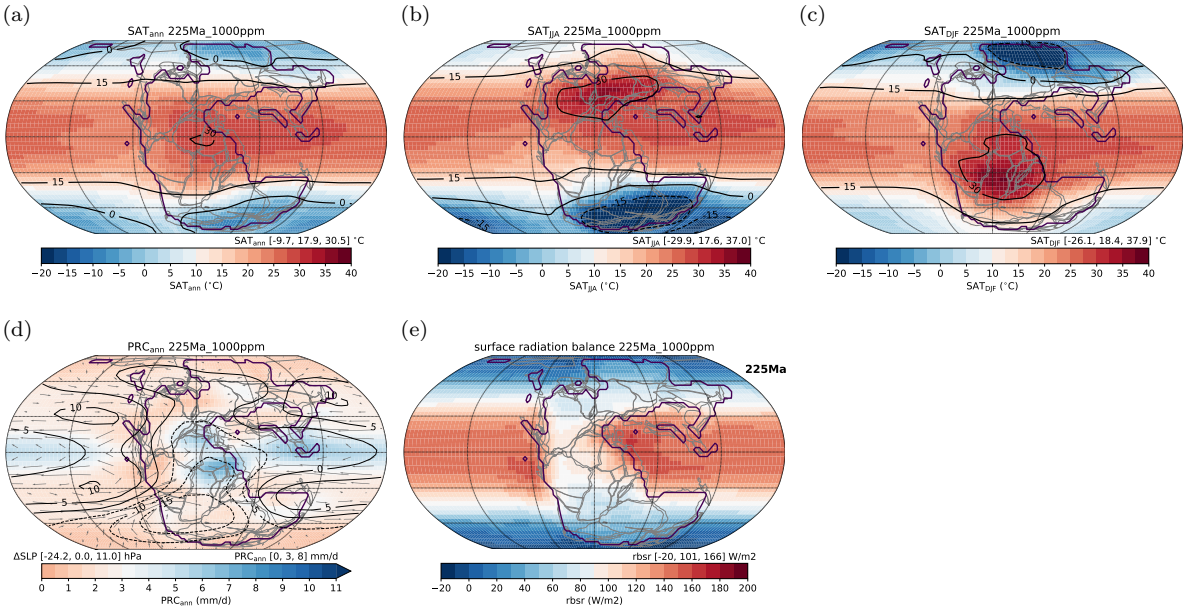

Figure S10. Same as Fig. S7 but at 225 Ma

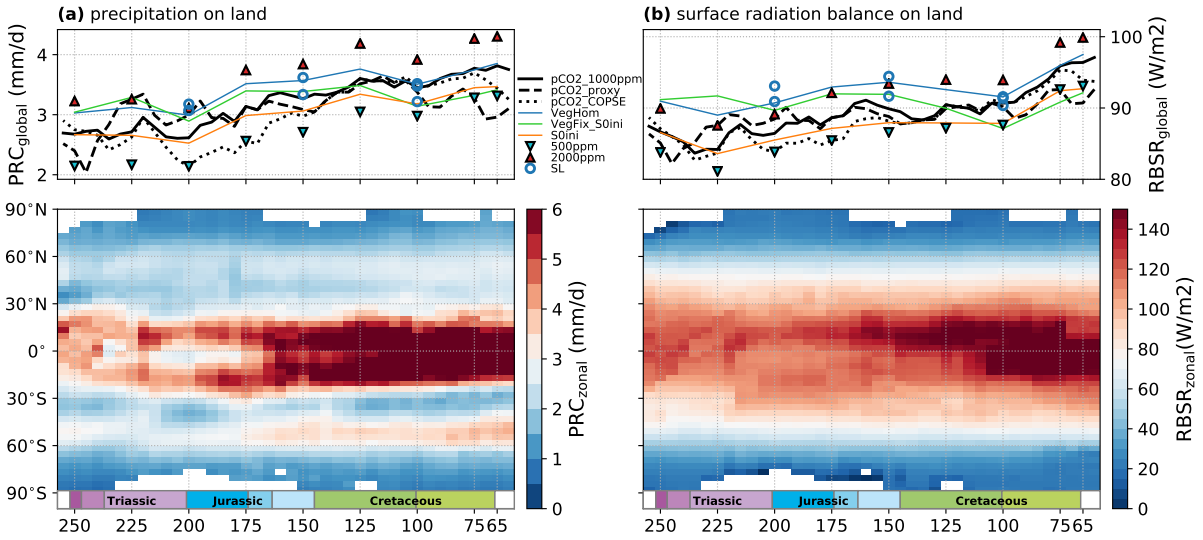

Figure S11. Zonal and global mean precipitation (a) and surface radiation balance (b) on land. Zonal mean values in the bottom panels are from the $\mathtt{P}_{\mathtt{pCO2\_1000ppm}}$ baseline pathway, while the top panels also include results from the other pathways.

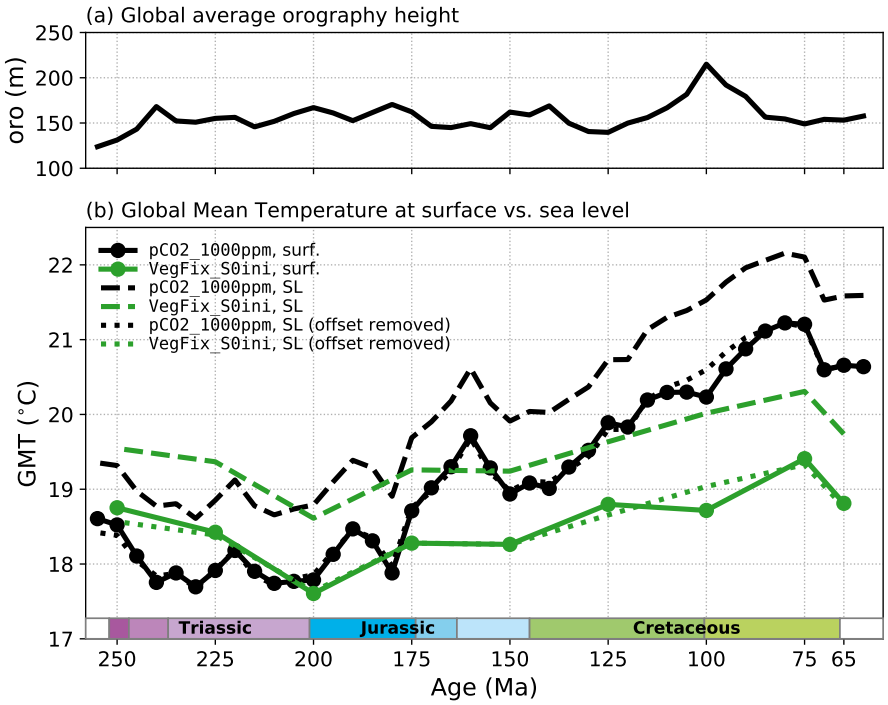

Figure S12. (a): Globally averaged height of the orography (Scotese & Wright, 2018) as implemented in the CLIMBER-3α model simulations. (b): Global mean surface air temperatures (GMST, solid lines) compared to lapse-rate corrected global mean temperatures at sea-level (dashed lines), for $\mathtt{P}_{\mathtt{pCO2\_1000ppm}}$ (black) and $\mathtt{P}_{\mathtt{VegFix\_S0ini}}$ (green). Dotted lines are also sea-level temperatures, but the offset to GMST at 150 Ma was removed to illustrate differences in the evolution through time.

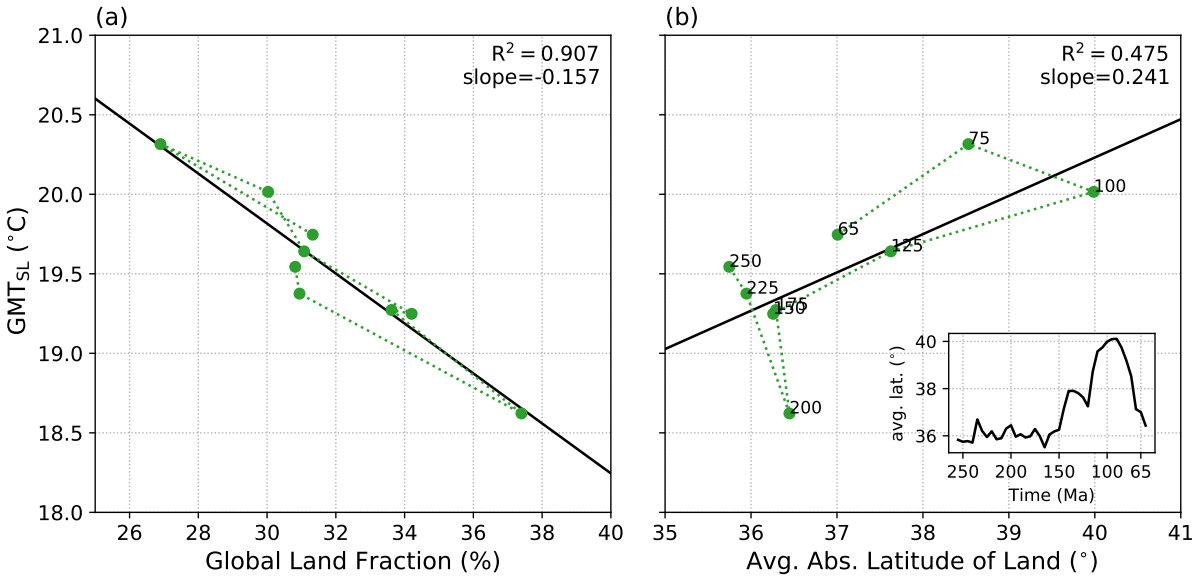

Figure S13. Correlation of lapse-rate corrected global mean air temperatures at sea level (GMT_{SL}) with (a) the global land area fraction and (b) the average absolute latitude of land area the time evolution of which is also shown in the inset. For the simulations of the $P_{\texttt{VegFix\_S0ini}}$ pathway.

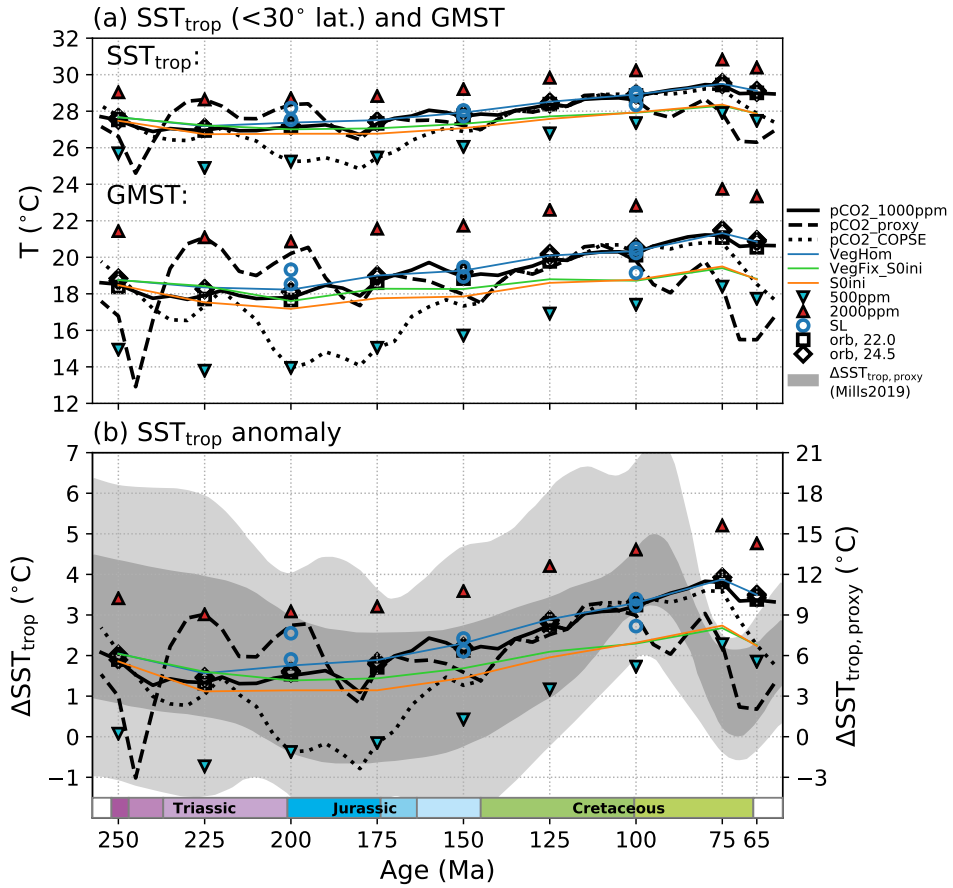

Figure S14. (a): Simulated global mean surface air temperatures and tropical sea surface temperatures (latitudes $< 30°$). (b): The gray shading indicates proxy-based tropical SST anomalies (ΔSST_{trop}, relative to the present) from (Mills et al., 2019). For this the GMST envelope from Mills et al. (2019, Fig. 4a) was scaled back to (ΔSST_{trop}) using Eq. 1 from the supplement to (Mills et al., 2019). Lines and markers indicate ΔSST_{trop} obtained for the CLIMBER-3α simulations, using the the scaling factor of 1.79 (as determined in Fig. S15). See Supp. Sec. 6 for further explanation.

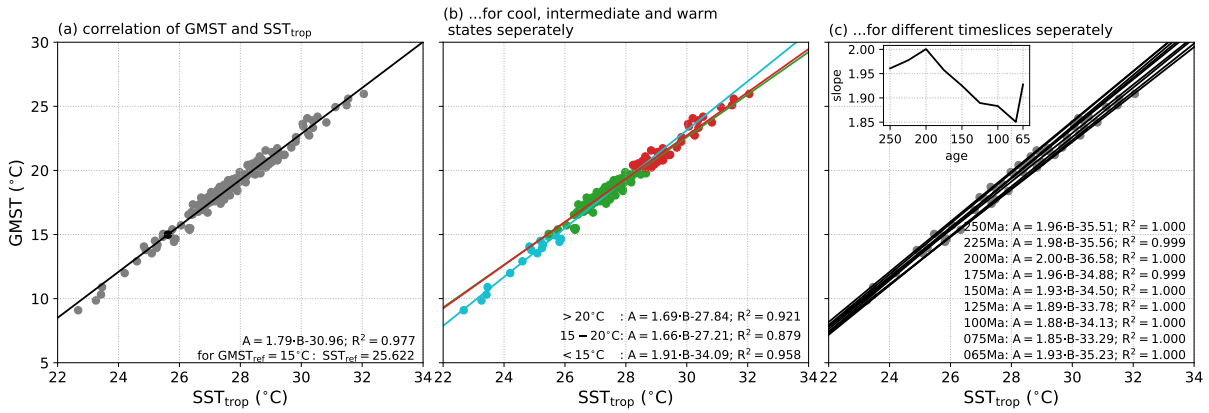

Figure S15. Correlation of simulated global mean surface air temperatures and tropical sea surface temperatures (latitudes $< 30°$). (a): For all simulations of the $\mathtt{P_{pCO2\_1000ppm}}$ pathway and all pCO_2 sensitivity experiments (each represented by one gray dot). (b): For cool (GMST $< 15\,°C$, cyan), intermediate ($15\,°C <$ GMST $< 20\,°C$, green) and warm (GMST $> 20\,°C$, red) states separately. (c): Separately for the $\mathtt{T_{25Myr}}$ timeslices including their climate states at $pCO_2 = [250, 500, 1000, 1500, 2000, 4000]$ ppm. The inset indicates the obtained scaling factor for these timeslices. See Supp. Sec. 6 for further explanation.

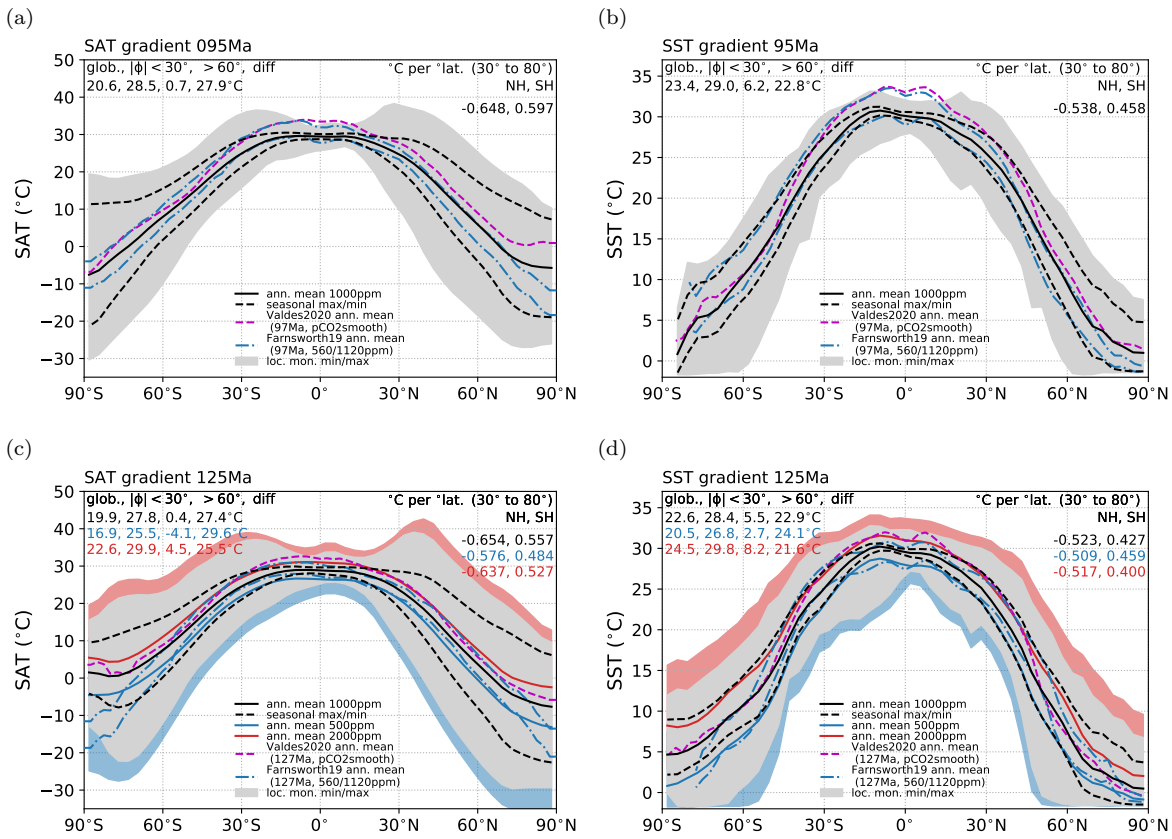

Figure S16. Simulated zonal mean SAT (left) and SST (right) profiles for the 95 and 125 Ma timeslices. For 1000ppm: annual mean (solid black line), seasonal min./max. (dashed black lines). For 500/1000/2000 ppm: monthly min./max. (blue/grey/red shading). Additionally annual mean for 500 ppm (solid blue line), 2000 ppm (solid red line), Valdes et al. (2020) data (dashed magenta line, `pCO2_smooth`), Farnsworth et al. (2019a) data (dashed blue line). Upper left corners: Numerical values of the global, low latitude (<30 °), high latitude (>60 °) averages and the difference between the latter two. Upper right corners: average meridional temperature gradient in °C per °lat. between 30 and 80 ° latitude. Similar plots for all 40 Mesozoic timeslices are included in the accompanying data repository (AllTimeslices_MeridionalGradient_SST.pdf and AllTimeslices_MeridionalGradient_SST.pdf).

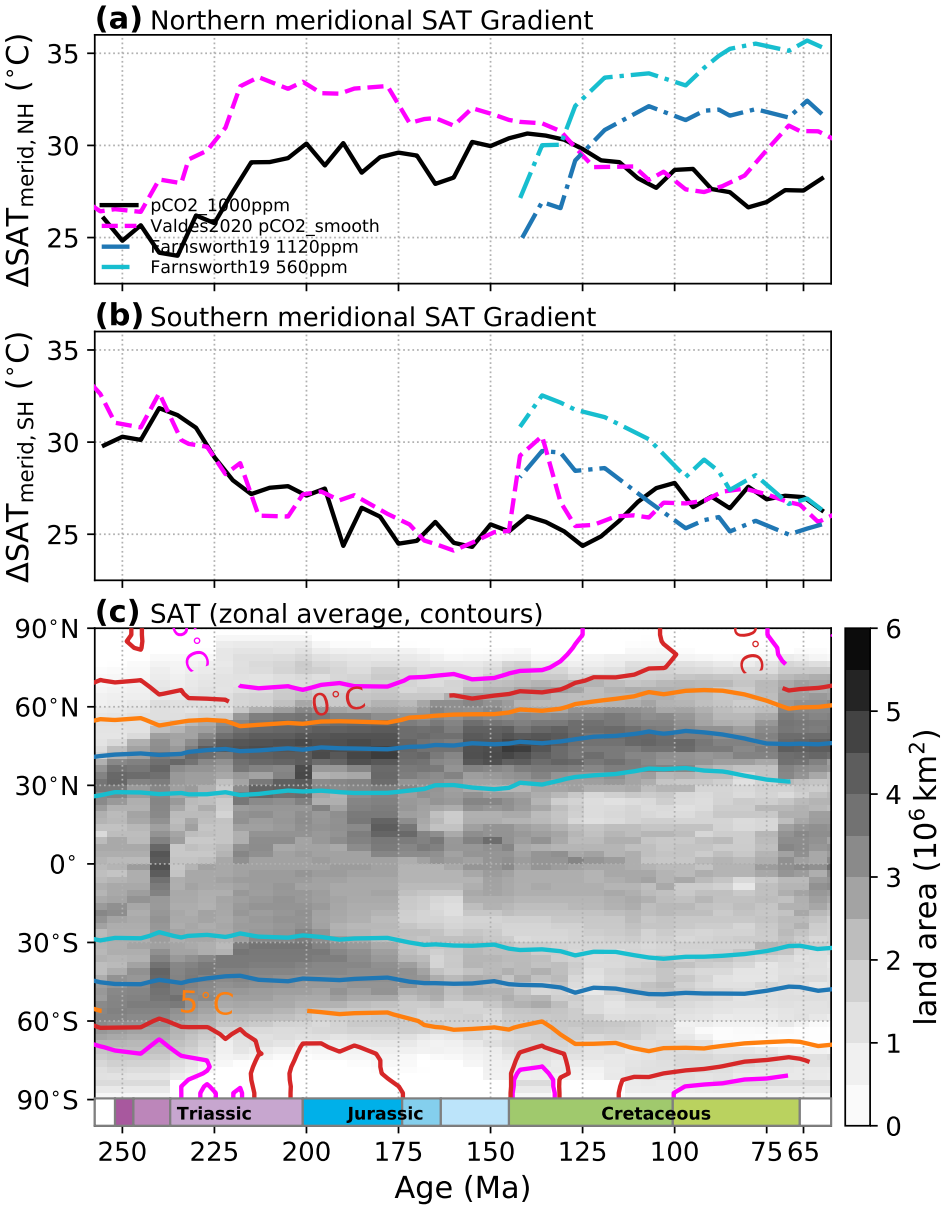

Figure S17. Evolution of simulated zonal mean Surface Air Temperatures (SAT, c) and the thermal contrast between low-latitude and northern (a) and southern (c) high-latitude regions for data from Valdes et al. (2020) and Farnsworth et al. (2019a). (For comparison with Fig. 5.) (c): Contours indicate annual zonal mean SAT for all runs of the `pCO2_smooth` pathway from Valdes et al. (2020). The grey shading indicates the changing latitudinal distribution of land area in the model paleogeographies. (a,b): Annual zonal mean SAT difference between low-latitude (<30 ° lat.) an northern (a) and southern (b) high-latitude regions (>60 ° lat.) through time.

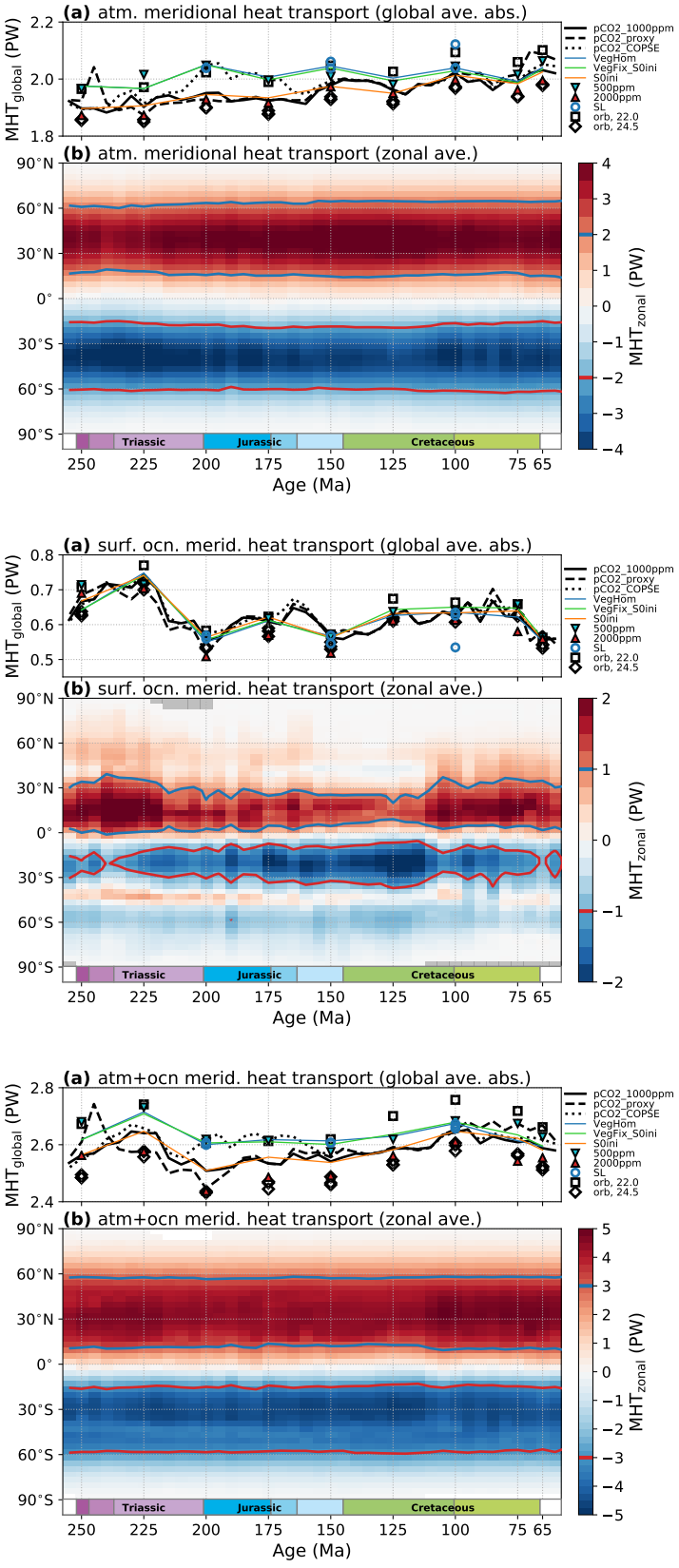

Figure S18. Meridional heat transport (MHT) by the atmosphere (top), ocean (middle) and in total (bottom). For the respective bottom panels, zonal mean values from all timeslices of the $\mathtt{P}_{\mathtt{pCO2\_1000ppm}}$ pathway have been aggregated. The upper panels indicate global mean values of the absolute MHT values.

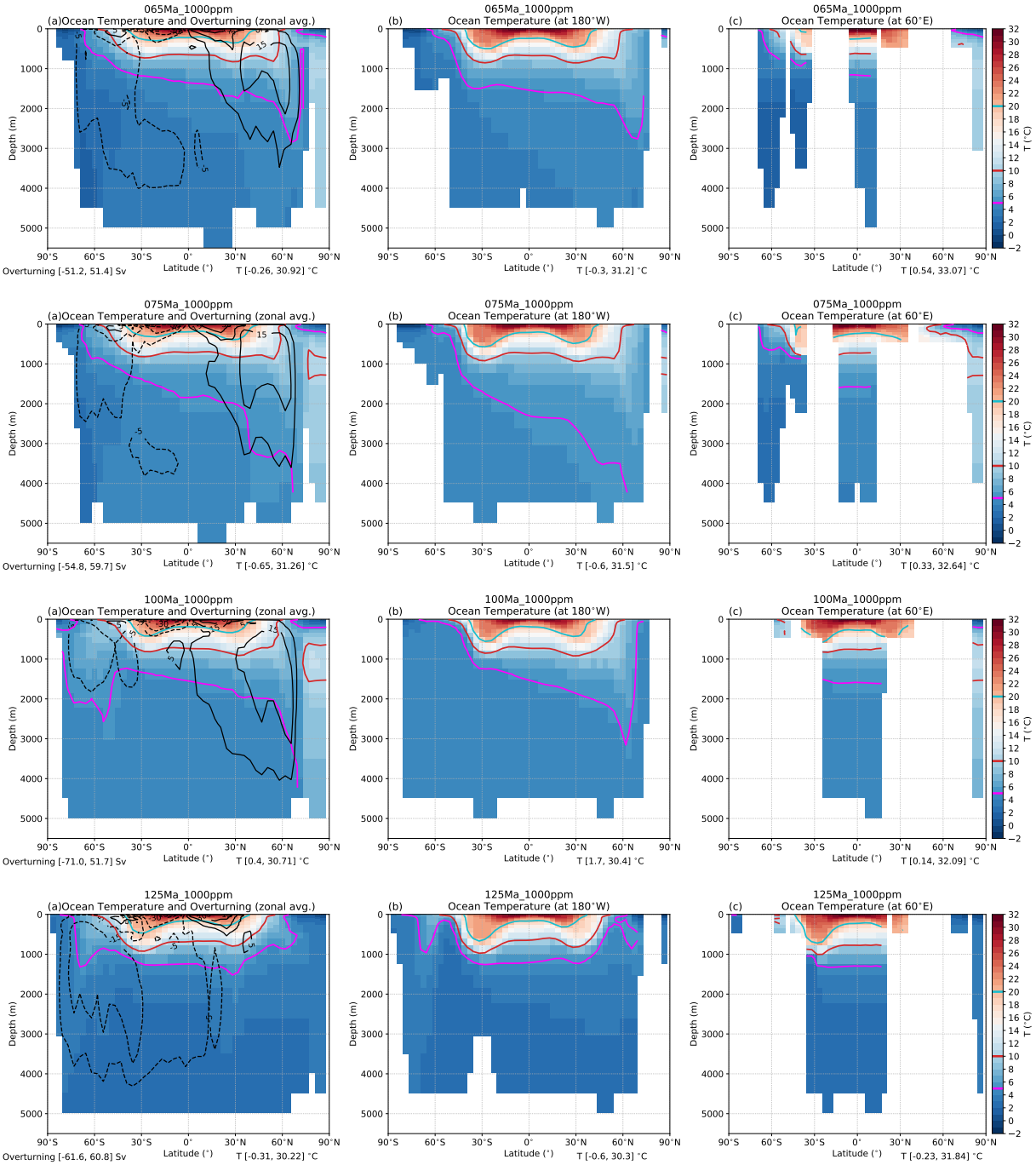

Figure S19. Meridional cross-sections showing the annual mean ocean temperatures as a zonal mean (a), at 180 °W (b) and 60 °E (c). In (a), the black contours indicate the global mean meriodional overturning streamfunction.

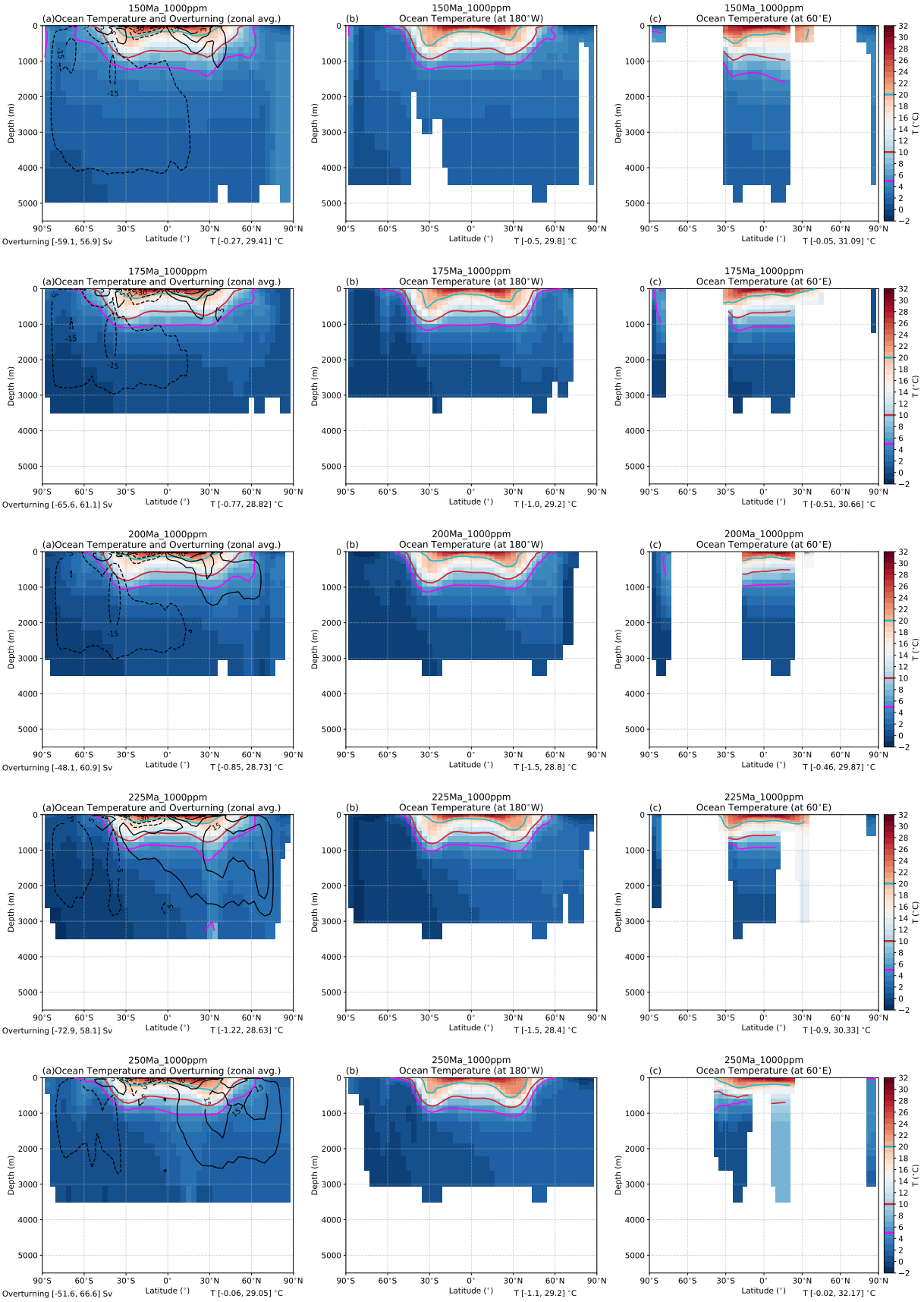

... Fig. S19 continued

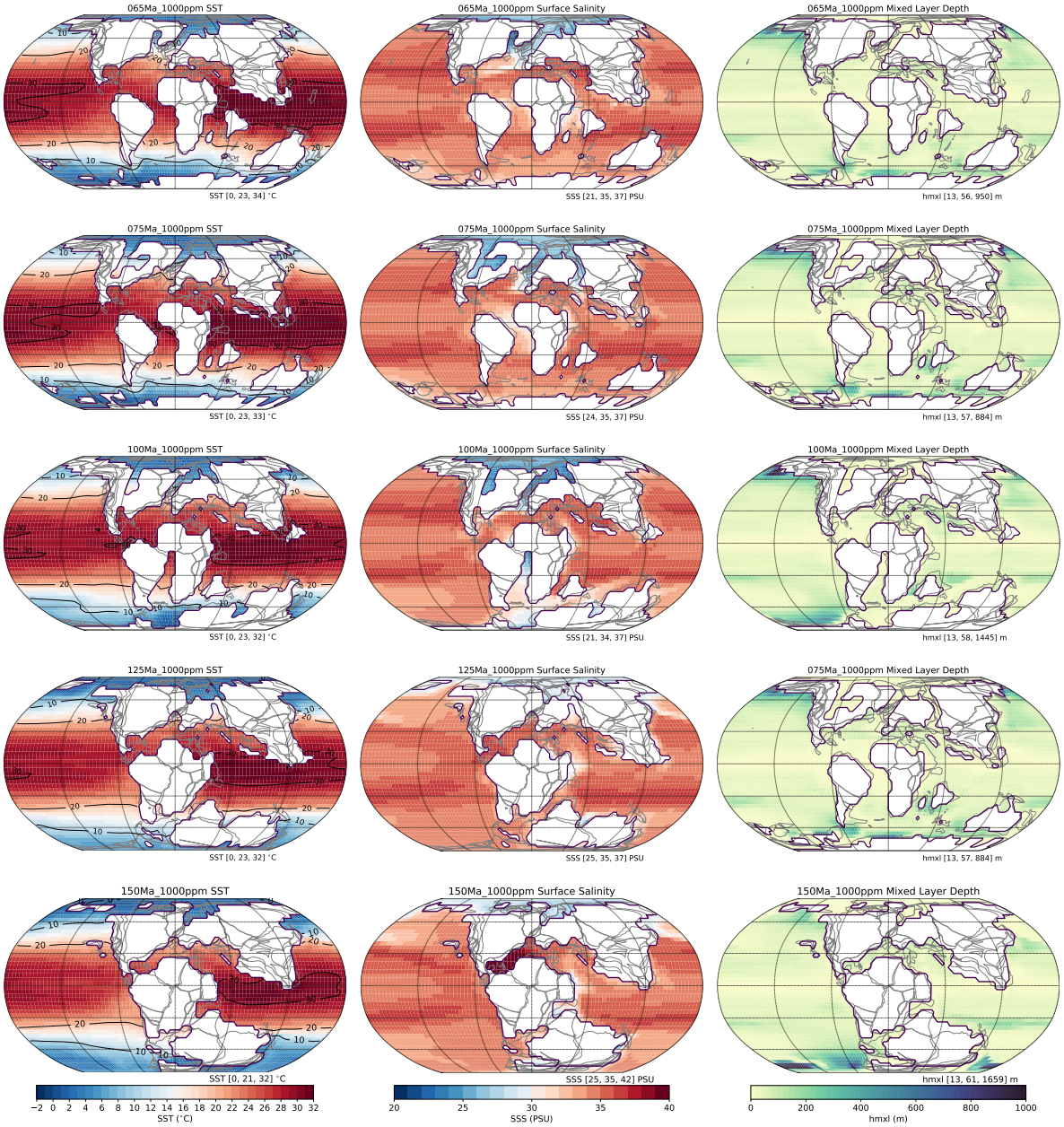

Figure S20. Annual mean Sea Surface Temperatures (left), Surface Salinity (middle) and Mixed Layer Depth (right). For the $\mathtt{P_{pCO2\_1000ppm}}$ pathway.

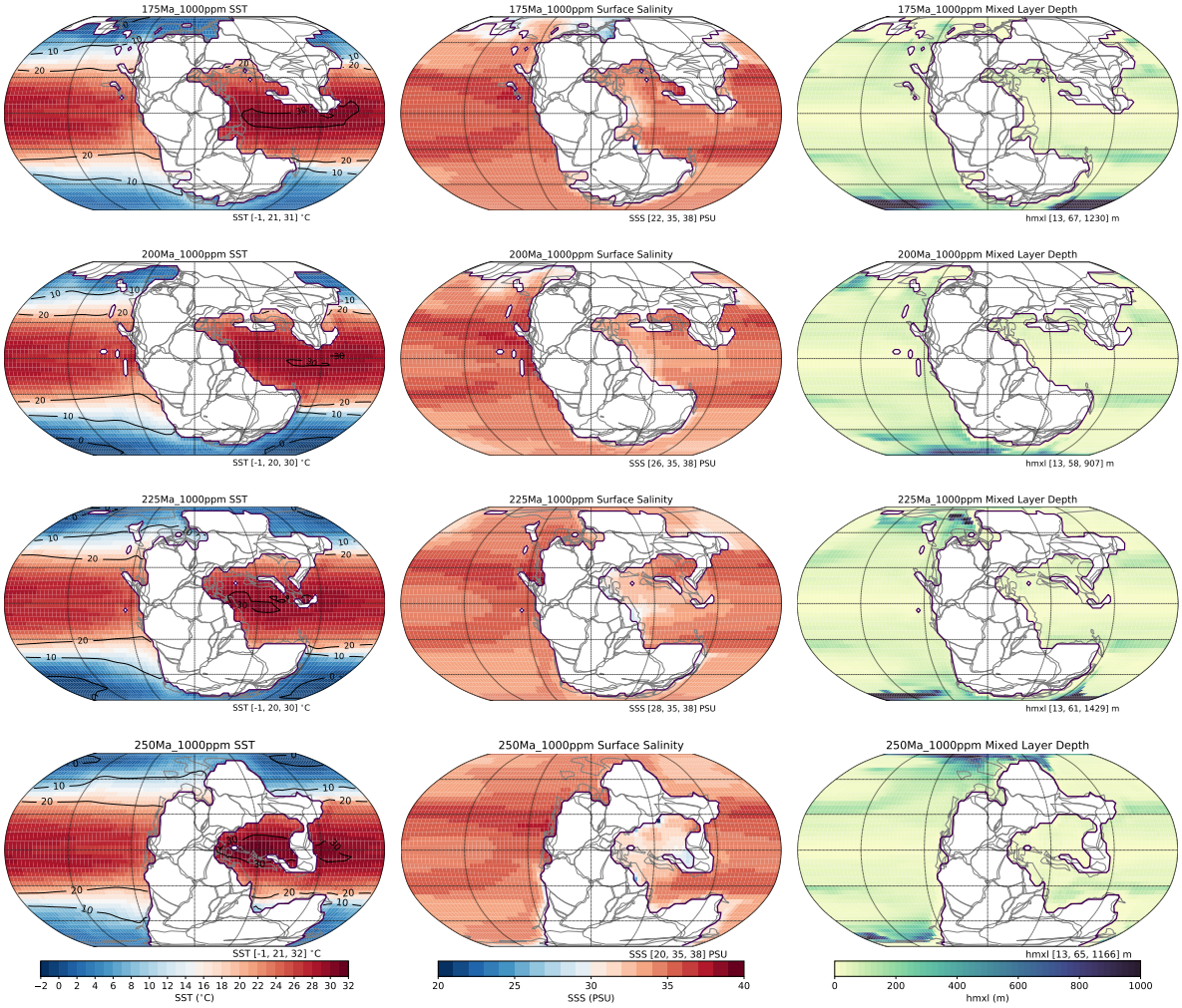

... Fig. S20 continued

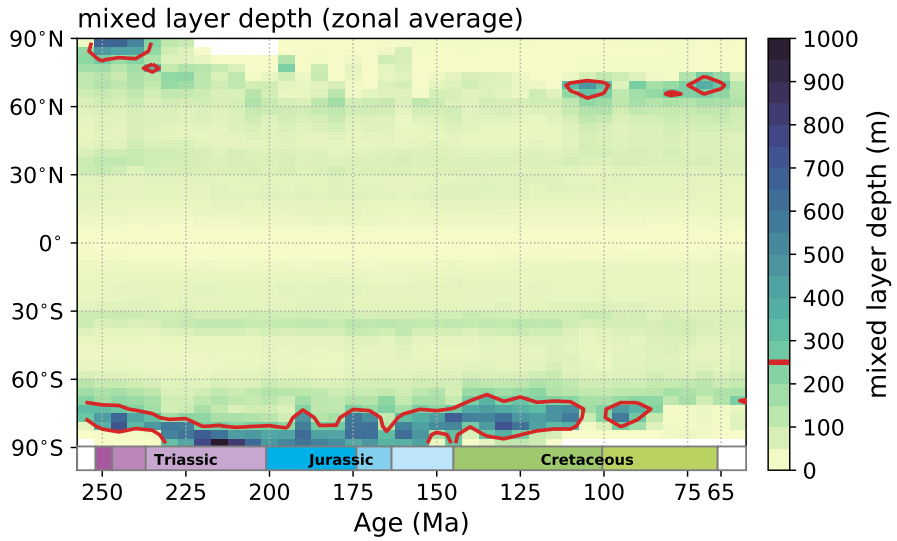

Figure S21. Zonal and annual mean mixed layer depth, aggregated for the simulations of the $P_{pCO2\_1000ppm}$ pathway.

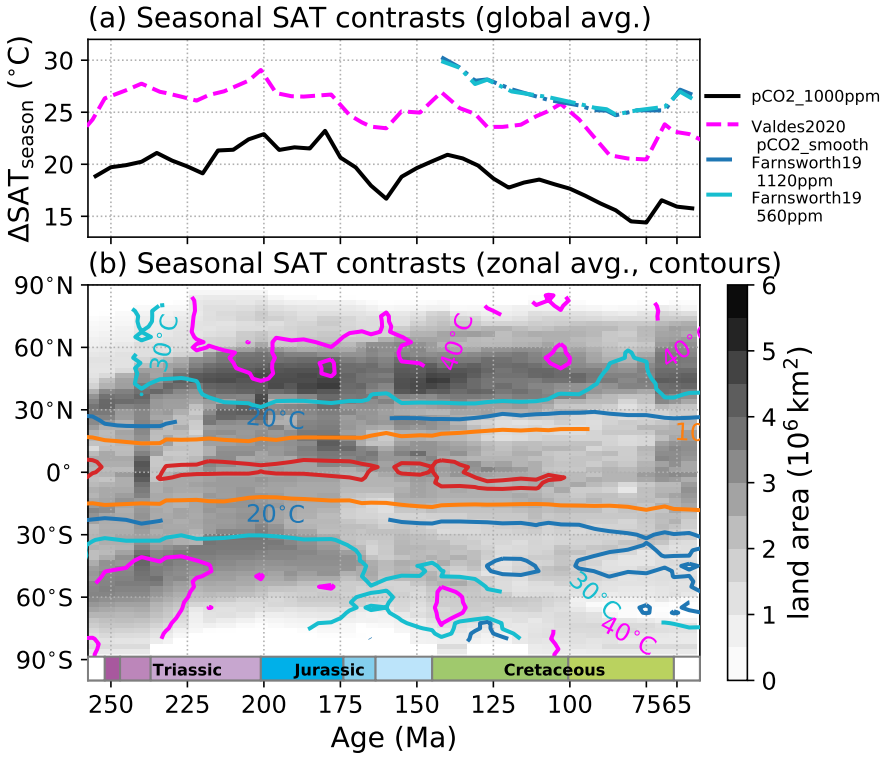

Figure S22. Simulated seasonality of surface air temperatures (SAT). With data from Valdes et al. (2020, P_{pCO2_smooth} pathway) and Farnsworth et al. (2019a) for comparison with the results from CLIMBER-3α presented in Fig. 3. (b): Zonal averages of the seasonal differences (max. difference between the DJF, MAM, JJA and SON seasonal averages) for all timeslices of the (Valdes et al., 2020) simulations (contours). The grey shading shows the changing latitudinal land area distribution implemented in the simulations. (a): Globally averaged continental SAT seasonality.